Published as J. Catal. 2016, 340, 30-40. doi.org/10.1016/j.jcat.2016.05.005

Highly Efficient and Selective Reduction of Nitroarenes into Anilines Catalyzed by Gold Nanoparticles Incarcerated in a Nanoporous Polymer Matrix: Role of the Polymeric Support and Insight into the Reaction Mechanism

*Annarita Noschese,[a†] Antonio Buonerba,[ab†] Patrizia Canton,[c] Stefano Milione,[ab] Carmine Capacchione[ab] and Alfonso Grassi[ab]**

[a] Dipartimento di Chimica e Biologia "Adolfo Zambelli", Università degli Studi di Salerno, via Giovanni Paolo II, 84084 Fisciano (SA), Italy.

[b] CIRCC, Interuniversity Consortium Chemical Reactivity and Catalysis, via Celso Ulpiani 27, 70126 (BA), Italy.

[c] Dipartimento di Scienze Molecolari e Nanosistemi, Università Ca' Foscari Venezia, Via Torino 155/B, 30170 Mestre (VE), Italy.

[†] These authors contributed equally.

* Corresponding author. E-mail: agrassi@unisa.it.

Published as J. Catal. 2016, 340, 30-40. doi.org/10.1016/j.jcat.2016.05.005

ABSTRACT

Gold nanoparticles supported onto a nanoporous semicrystalline polymorphic polymer matrix consisting of syndiotactic polystyrene-*co*-*cis*-1,4-polybutadiene multiblock copolymer (AuNPs-sPSB) were investigated as catalyst in the reduction of nitroarenes into anilines using sodium borohydride as reductant. The crystalline phase and the morphology of the polymeric support were varied to assess their influence on the selectivity of the reaction pathway. The β and γ crystalline forms, which are not permeable to small molecules, led to a partial reduction of nitrobenzene into both azoxybenzene and diazobenzene whereas the porous δ and ε crystalline forms efficiently catalyze the complete reduction into aniline through the *condensation route* of the reaction mechanism proposed by Haber, achieving the highest activities reported so far for this reaction.

KEYWORDS:

Gold Nanoparticles; Nitroarene reduction; Porous polymers; Mechanism; Azocompounds; Heterogeneous catalysis

HIGHLIGHTS

- Gold nanoparticles hosted into a porous polymorphic polymer matrix as catalyst.
- Efficient and selective reduction of nitroarenes to anilines under mild conditions.
- Crystallinity and nanoporosity of the support assist the catalytic process.
- Insights on kinetics and on the reaction mechanism.
- The nitroarene reduction follows the *condensation route* of the mechanism of Haber.

Published as J. Catal. 2016, 340, 30-40. doi.org/10.1016/j.jcat.2016.05.005

GRAPHICS FOR TABLE OF CONTENTS

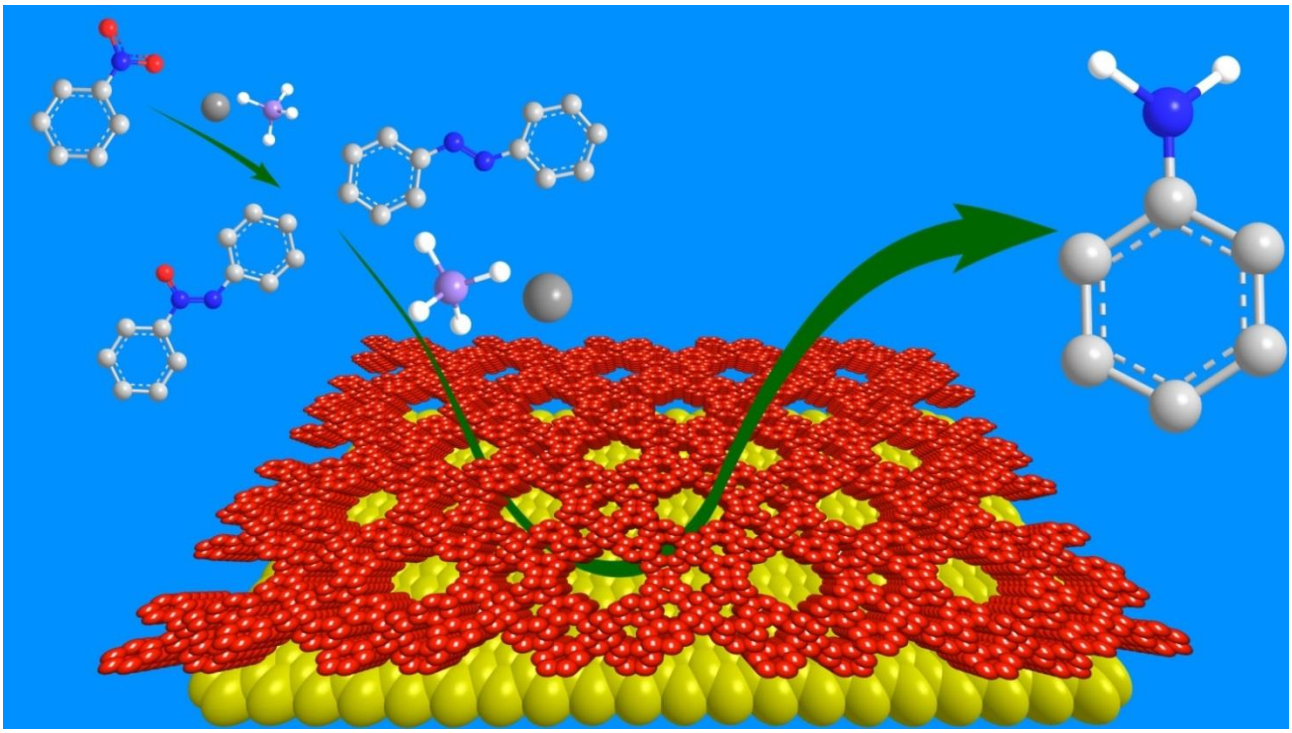

Published as J. Catal. 2016, 340, 30-40. doi.org/10.1016/j.jcat.2016.05.005

1. INTRODUCTION

Gold Nanoparticles (AuNPs) stabilized by inorganic supports or embedded into polymer matrices are emerging as a powerful tool in sustainable catalysis. Following the pioneering studies of Haruta on the low temperature oxidation of carbon monoxide to carbon dioxide catalyzed by AuNPs supported onto transition metal oxides using dioxygen as oxidant, a variety of aerobic oxidation reactions have been successfully carried out under very mild conditions and with high efficiency and selectivity.[1] The reaction mechanism is currently matter of debate, but some features seem, to date, well assessed and commonly accepted.[1e,2] A hydride shift from the substrate to be oxidized to the surface of the AuNPs produces the Au-H species that initiates the specific cascade of reactions leading to the oxidation of the targeted molecule: this reaction is considered the rate determining step, as extensively demonstrated by isotope kinetic measurement, EPR spectroscopy of the catalyst solution under aerobic conditions, and Hammet plots.[2a,f,3] DFT calculations substantiated this reaction pathway, initially proposed on the basis of a number of experimental evidences.[2b,f,4] Actually labeling experiments using $^{18}O_2$ showed no incorporation of the isotopomer in the oxidation products to confirm that dioxygen acts just as hydride scavenger from the AuNPs surface to produce the hydroperoxo species, Au-OOH, that in turn decomposes to hydrogen peroxide by protonolysis.[5] Interestingly the possibility of obtaining stable Au-H intermediate species paved the way to gold catalysts suitable for reduction reactions. Corma *et al.* first showed that AuNPs supported onto TiO_2 or Fe_2O_3 allow reduction of nitroaromatics into the corresponding anilines using molecular dihydrogen under harsh conditions (100-130 °C, 10-25 bars of H_2, 1-9 h).[6] The chemoselective hydrogenation of nitroaromatics comprising reducible functional groups, as *e.g.* nitrostyrene, nitrobenzaldehydes and nitrobenzonitriles, was thus successfully accomplished. Other authors showed later that the reaction could be carried out under milder conditions using alternative and more efficient reductants as the ammonia-borane complex,[7] sodium borohydride,[8] isopropanol,[9] silanes,[10] CO/H_2O[11] (WGS reaction as source of dihydrogen). Intriguingly UV-Vis light irradiation of the AuNPs - TiO_2 catalysts produced the selective reduction of nitrobenzenes to azobenzenes.[12]

AuNPs seem to mimic biological enzymes, namely nitroreductases, which catalyze the reduction of nitrocompounds using flavin mononucleotide (FMN) or flavin adenine dinucleotide (FAD) as prosthetic groups, and nicotinamide adenine dinucleotide (NADH) or nicotinamide adenine dinucleotide phosphate (NADPH) as hydride donors.[13] The sequential bi-electron transfer from NAD(P)H results into the formation of the nitroso and hydroxylamine derivatives, and finally of the primary amine.[14] The presence of the hydroxylamino intermediate is well-established and proven in a number of studies; on the contrary, nitrosobenzene is extremely reactive and its bi-electron reduction is so fast that this species cannot be isolated or detected. The cascade of reaction intermediates in the bioreduction of nitroaromatics is analogue to that proposed in the Haber mechanism as direct route catalyzed by noble metals (*vide infra*; Scheme *1*).

We have recently reported that AuNPs embedded into a nanoporous crystalline polymer matrix consisting of the syndiotactic polystyrene-*cis*-1,4-polybutadiene multiblock copolymer (AuNPs-sPSB) efficiently catalyze the selective aerobic oxidation of primary and secondary allyl, and of benzyl and *benzyl like* alcohols, to the corresponding aldehydes and ketones, leaving alkyl alcohols not reacted.[15] These findings allowed the efficient and selective synthesis of alkyl cinnamates via the in situ aerobic oxidative esterification of cinnamyl alcohols with alkyl alcohols.[16,17] The

Published as J. Catal. 2016, 340, 30-40. doi.org/10.1016/j.jcat.2016.05.005

polymer host matrix of AuNPs-sPSB mainly consists of syndiotactic polystyrene, a semicrystalline thermally stable and chemically inert polymorphic polymer that exhibits five crystalline forms, namely α, β, γ, δ and ε.[18] While the α, β, γ polymer phases are poorly permeable to small organic molecules, the δ and ε crystalline forms are nanoporous and include, in the crystalline lattice, nanovoids and nanochannels respectively; a variety of halogenated and aromatic molecules can be therein hosted, producing *co*-crystals and intercalate structures, respectively.[19] The remarkable activity and selectivity of the AuNPs-sPSB catalyst in oxidation catalysis was attributed to the porosity of the ε form of the polymeric support which allows fast and selective diffusion of the reactants to the catalytic active sites.[15,16] These seminal and encouraging results prompted us to definitively demonstrate the effectiveness of this nanoporous host polymer matrix in other examples of redox reactions catalyzed by AuNPs. Considering that both nitrobenzenes[20] and azobenzenes[21] produce stable co-crystals with the δ and ε forms of syndiotactic polystyrene we decided to explore the reduction of nitroaromatics using the AuNPs-sPSB catalyst and $NaBH_4$ as reductant, aiming also to elucidate the reaction pathway.

2. EXPERIMENTAL SECTION

General procedures and materials. The manipulation of air- and moisture-sensitive compounds was performed under nitrogen atmosphere using standard Schlenk techniques and an MBraun glovebox. Toluene (99.5%) was dried over calcium chloride, refluxed for 48h over sodium and finally distilled before use in moisture- and oxygen-sensitive reactions. Tetrahydrofuran (99.5%) was dried over potassium hydroxide, refluxed for 48h over Na/benzophenone and distilled before use in the synthesis of the catalyst. Styrene (99%) was purified by stirring for 12 h over calcium hydride before distillation under reduced pressure. Tetrachloroauric acid trihydrate (≥49.0% Au basis), sodium triethylborohydride (1.0 M in THF), water (HPLC grade), methanol (HPLC grade), ethanol (≥99.8%), ethylene glycol (≥99%), 1-propanol (≥99.5%), 1-butanol (98%), acetone (≥99%), sodium borohydride (>98%), anisole (99%), nitrobenzene (>99.5%), 4-nitrobenzyl alcohol (99%), 4-nitrobenzaldehyde (98%), 4-nitroaniline (≥99%), 4-nitrotoluene (99%), 4-nitroanisole (99%), 4-chloronitrobenzene (99%), 1,2-dichloro-4-nitrobenzene (99%), 4-nitrobenzoic acid (>98%), 4-nitrophenol (≥99%,) were purchased from commercial sources (Carlo Erba, TCI, Sigma-Aldrich, Labscan and Romil) and used as received. Deuterated solvents were purchased from Euriso-Top or Sigma–Aldrich and used as received.

Instrumentation and methods. The NMR characterization of the reaction products was performed on Avance Bruker spectrometers (600, 400, 300 and 250 MHz for ^1H) using the following ^1H NMR diagnostic signals: 4-aminobenzyl alcohol [(300 MHz, CD_2Cl_2): 7.04 (d, 2H, J=8.0 Hz), 6.60 (d, 2H, J=8.0 Hz), 4.40 (s, 2H), 3.52 (br s, 2H)]; 4-aminoaniline [(250 MHz, CD_2Cl_2), 6.55 (s, 4H), 3.77 (br s, 2H)]; 4-toluidine [(400 MHz, CD_2Cl_2), 6.86 (d, 2H, J=8.0 Hz), 6.55 (d, 2H, J=8.2 Hz), 3.88 (br s, 2H), 2.14 (s, 2H)]; 4,4'-dimethoxyazobenzene [300 MHz, CD_2Cl_2), 8.16 (m, 4H), 6.92 (m, 4H), 3.79 (s, 6H)]; 4-anisidine [(300 MHz, CD_2Cl_2), 6.6 (m, 4H), 3.64 (s, 3H), 3.55 (br s, 2H)]; 4,4'-dichloroazoxybenzene [(300 MHz, CD_2Cl_2): 8.19 (d, 2H, J= 8.4 Hz), 8.10 (d, 2H, J=8.8 Hz), 7.45 (d, 2H, J=8.4 Hz), 7.39 (d, 2H, J=8.8 Hz)]; 4-chloroaniline [(300 MHz, CD_2Cl_2): 6.95 (d, 2H, J= 8.7 Hz), 6.59 (d, 2H, J= 8.7 Hz), 3.55 (br s, 2H)]; 3,3',4,4'-tetrachloroazobenzene [(250 MHz, CD_2Cl_2): 7.94 (d, 2H, J= 2.1 Hz), 7.75 (dd, 2H, J_1= 8.4 Hz, J_2= 2.4 Hz), 7.57 (d, 2H, J=8.4 Hz)];

Published as J. Catal. 2016, 340, 30-40. doi.org/10.1016/j.jcat.2016.05.005

1,2-bis(3,4-dichlorophenyl)hydrazine [(250 MHz, CD_2Cl_2): 7.13 (d, 2H, J= 8.8 Hz), 6.87 (d, 2H, J= 2.6 Hz), 6.63 (dd, 2H, J_1=8.8 Hz, J_2= 2.6 Hz)]; 1,2-chloro-4-aniline [(250 MHz, CD_2Cl_2): 7.05 (d, 1H, J= 8.6 Hz), 6.71 (d, 1H, J= 2.7 Hz), 6.48 (dd, 1H, J_1=8.6 Hz, J_2= 2.7 Hz), 3.59 (br s, 2H)]. WAXD patterns were obtained in reflection mode with an automatic Bruker D8 powder diffractometer using the Ni-filtered Cu K_α radiation. TEM analysis were carried out with a JEOL (JEM 3010) electron microscope operating at 300 kV, with a point-to-point resolution of 0.17 nm (at Scherzer defocus). Specimens were sonicated in 2-propanol, and then transferred (10 mL) onto a copper grid covered with a lacey carbon film supplied from Assing. The size distribution profile of the AuNPs was manually calculated using the software Photoshop CC2014. SEM analysis was carried out with a scanning electron microscope (Zeiss Sigma-VP FE-SEM). AAS analysis was performed on a PerkinElmer AAnalyst 100 spectrophotometer using an Au hollow cathode lamp (Perkin–Elmer). ICP-OES was performed on a Perkin–Elmer Optima 7000 DV instrument. GC-MS analysis were carried out on a GC-MS 7890A/5975C chromatograph from Agilent Technologies equipped with an DB 17MS column (phenyl/methyl-polysiloxane, 30 m, 0.25 mm ID) and a mass-selective detector. The surface areas of the polymer matrix were determined by nitrogen absorption at 77 K of the AuNPs-sPSB powders degassed at 40°C under vacuum for 24h using a Nova Quantachrome 4200e. The specific surface area was calculated using the BET method.

Synthesis of the Au-Cδ, Au-Cβ, Au-Cγ and Au-Cε catalysts. The multiblock syndiotactic polystyrene-*co*-1,4-*cis*-polybutadiene copolymer (sPSB) and the corresponding catalysts **Au-Cδ, Au-Cβ, Au-Cγ and Au-Cε** (the greek symbol stands for the crystalline form of the host polymer phase) were synthesized as previously reported.[15,16,22] Briefly: a 1 L round-bottomed three-necked flask equipped with a magnetic stirring bar was charged with anhydrous THF (650 mL) and finely grounded sPSB (4.9 g; x_S= 0.88). The mixture was stirred for 24 h at room temperature and then heated to reflux for 1 h to reach the complete swelling of the polymer. $HAuCl_4 \cdot 3H_2O$ (0.210 g; 0.56 mmol) was added at room temperature and the resulting slurry kept under stirring for 24 h, then refluxed for 1h. A THF solution of sodium triethylborohydride (10 mL, 1.0 M) was added at 25 °C producing a rapid change of the color from pale yellow to red. The polymer was rapidly coagulated in a plenty of methanol, recovered by filtration, washed with fresh methanol and dried in vacuo at room temperature. The resulting catalyst **Au-Cδ** was analyzed by AAS and ICP-OES to assess the gold content of 2% *w/w*. The annealing of **Au-Cδ** at 170°C for 5h, or at 135°C for 2h led to **Au-Cβ** and **Au-Cγ**, respectively. The **Au-Cε** catalyst was obtained by stirring **Au-Cβ** in $CHCl_3/H_2O$ (*v*/*v* = 1/1) for 24 h at room temperature.

Reduction of nitrobenzene (NB) catalyzed by Au-Cδ, Au-Cβ, Au-Cγ and Au-Cε. A typical procedure is herein given (entry **4** of Table 1**)**. The Au-catalyst (50 mg; 2%w/w_{Au}), methanol (6 mL), nitrobenzene (2.54 mmol), anisole as internal standard (0.51 mmol) and $NaBH_4$ (15.2 mmol) were added in the order in a 50 mL round-bottom flask equipped with a condenser under N_2 at atmospheric pressure. The mixture was stirred at 35°C and aliquots of the reaction mixture were sampled at the desired reaction time. The catalyst was separated by filtration and the filtrate analyzed by GC-MS and NMR spectroscopy. At the end of reaction, the polymer was coagulated in a plenty of methanol, the catalyst recovered by filtration and the filtrate analyzed by GC-MS and ^{1}H-NMR.

Published as J. Catal. 2016, 340, 30-40. doi.org/10.1016/j.jcat.2016.05.005

3. RESULTS AND DISCUSSION

Synthesis and characterization of the Au-Cδ, Au-Cβ, Au-Cγ and Au-Cε catalysts. All of the AuNPs-sPSB catalysts used in this study resulted from a single batch synthesized according to the method previously described.[15,16] Briefly, the appropriate amount of sodium triethylborohydride was rapidly added to a THF solution of $HAuCl_4$ and sPSB (styrene content of 88 *mol*%) affording a slurry of the gold colloids stabilized by the polymer matrix. The polymer was rapidly coagulated in a plenty of methanol, filtered and dried. The gold concentration (2 % *w/w*) was determined by atomic absorption spectroscopy (AAS) and inductively coupled plasma optical emission spectrometry (ICP-OES) analysis. The powder wide angle x-ray diffraction (WAXD; Figure 1) spectra of the polymer host phase evidenced the presence of crystalline domains of syndiotactic polystyrene in the δ crystalline form (catalyst **Au-Cδ)** containing THF molecules clathrated in the cavities. The Scherrer[23] method applied to the <111> reflection of the crystalline AuNPs at 2θ = 38.2° allowed evaluating an average particle size of 4.9 nm (Figure 1a), in good agreement with the narrow size distribution centered at 5.0 nm found in the corresponding transmission electron microscopy (TEM) micrograph (see Figure 2a). The annealing of **Au-Cδ** at 170°C for 5h, or at 135°C for 2h led to **Au-Cβ** and **Au-Cγ**, respectively; the corresponding WAXD spectra are given in Figure 1b-c. After the thermal treatment, the average size of the AuNPs increased to 8.0 nm and 6.9 nm for **Au-Cβ** and **Au-Cγ,** respectively.

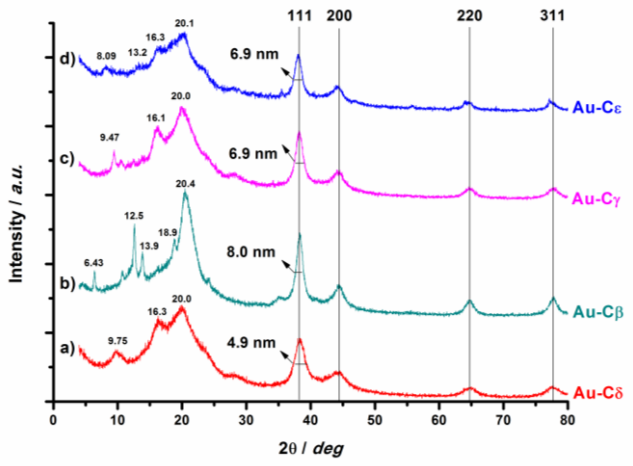

Figure 1. WAXD spectra of: a) **Au-Cδ**; b) **Au-Cβ**; c) **Au-Cγ**; d) **Au-Cε**. The size of the AuNPs was determined by the Scherrer method using the <111> reflection of the crystalline AuNPs at 2θ =38.2°.

The **Au-Cε** catalyst was prepared by stirring **Au-Cβ** in the mixture of solvents chloroform/water (1:1 v/v) at room temperature; the average size of the AuNPs resulted in this case slightly affected by the swelling of the polymer matrix in the halogenated solvent (Figure 1d).[24] The TEM micrographs of **Au-Cδ, Au-Cβ**, **Au-Cγ** and **Au-Cε** showed that the AuNPs are homogeneously dispersed in the polymer matrix and nanoparticles aggregates are not formed after the thermal treatments or the solvent swelling. Noteworthy the polymer phase surrounding the AuNPs in **Au-Cε**

Published as J. Catal. 2016, 340, 30-40. doi.org/10.1016/j.jcat.2016.05.005

is highly crystalline as evidenced by the selected area electron diffraction (SAED) reported in Figure 2d.

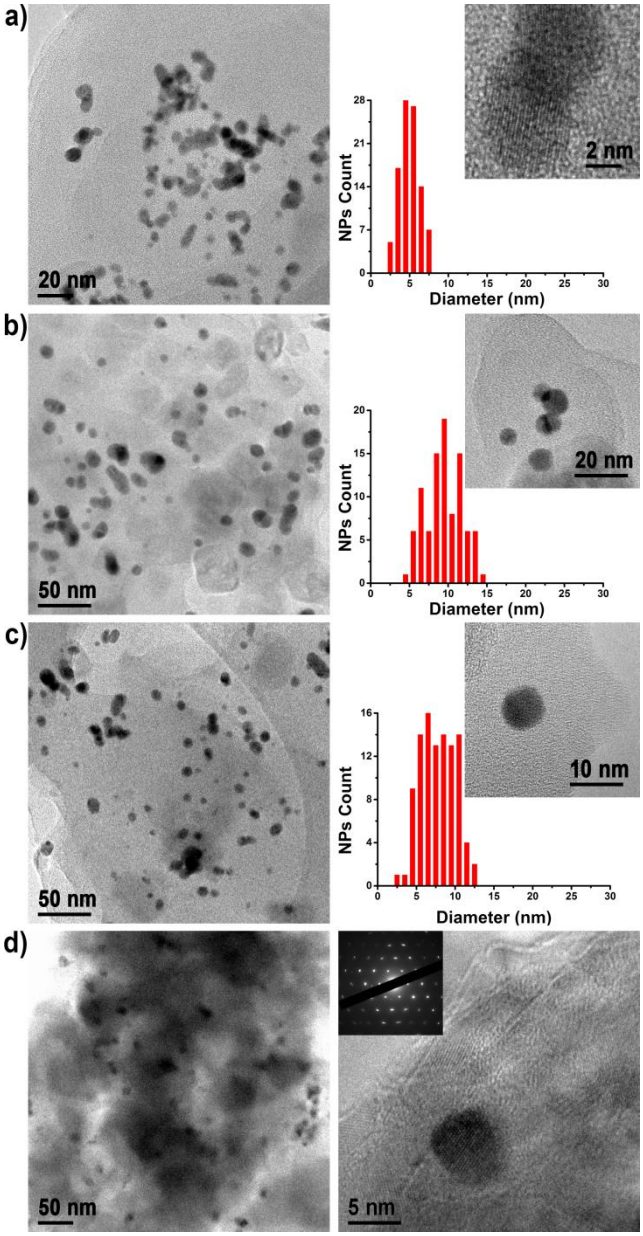

Figure 2. TEM micrograph (on the left) and the zoom in showing single AuNP and the corresponding size distribution profile (on the right) of: a) **Au-Cδ**; b) **Au-Cβ**; c) **Au-Cγ**; d) **Au-Cε**. The SAED in d) highlights the high degree of crystallinity of the polymer matrix surrounding the AuNPs in **Au-Cε**.

The polymeric support was investigated by scanning electron microscopy (SEM) and Brunauer-Emmet-Teller (BET) method[25] to assess the morphology and porosity of the polymer host phase after the thermal and solvent annealing. The SEM image of the **Au-Cδ** catalyst revealed a finely divided structure consisting of globular polymer particles sized in the micrometer scale (Figure 3a),

Published as J. Catal. 2016, 340, 30-40. doi.org/10.1016/j.jcat.2016.05.005

whereas the thermal treatment produced compact corrugated polymer grains of hundreds of micrometers in size for **Au-Cβ** and **Au-Cγ** (Figure 3b and 3c). The swelling of the polymer particles in water/chloroform, used for transforming **Au-Cβ** into **Au-Cε**, partially regenerated the pristine morphology observed in **Au-Cδ** (Figure 3d). The elaboration of the BET profiles (Figure S1-3) allowed to assign a surface area value of 16 m^2/g, 3.9 m^2/g and 24 m^2/g to **Au-Cδ**, **Au-Cγ** and **Au-Cε**, respectively, in agreement with the different packing of the crystalline phases.

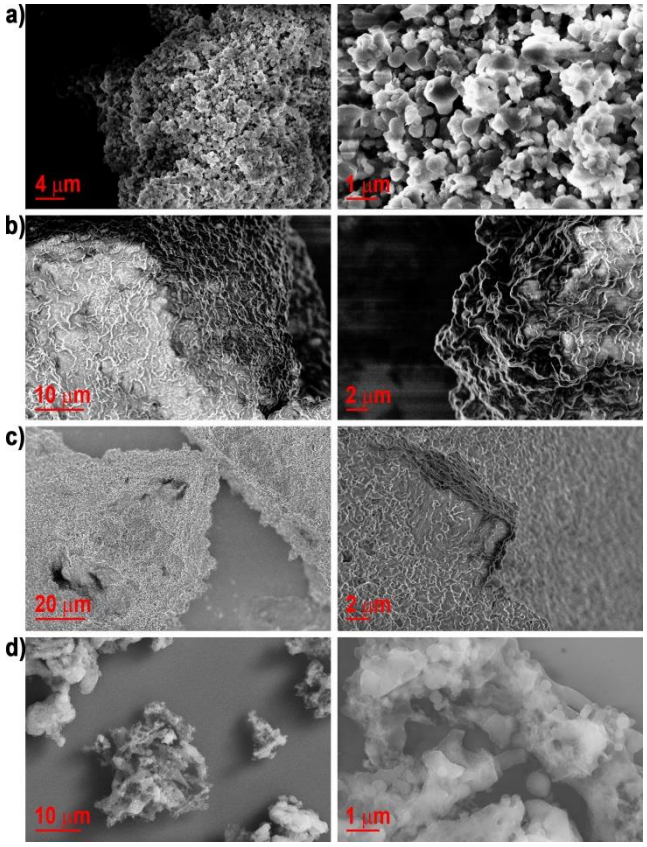

Figure 3. SEM micrograph of catalyst: a) **Au-Cδ**; b) **Au-Cβ**; c) **Au-Cγ** and d) **Au-Cε**.

Reduction of nitroarenes. Aromatic amines are important building blocks for the synthesis of amides, imines, azo-compounds, isocyanates and diazonium salts which are of value in a variety of applications, such as the synthesis of polymers, dyes, additives, agrochemicals and pharmaceuticals.[26,27] The most convenient synthetic route leading to aromatic amines is the nitroaromatics reduction; thus the quest for simple, green and effective reductive pathways of these compounds is of high interest in green and sustainable chemistry. Among the reductants, $NaBH_4$ is a cost effective and green reagent since it produces borates as non-toxic, easily disposable or regenerable by-products.[26b]

The reduction of nitrobenzene (**NB**) with $NaBH_4$ catalyzed by **Au-Cδ**, **Au-Cβ**, **Au-Cγ** and **Au-Cε** was preliminary screened in methanol under the mild reaction conditions of Table 1. Noteworthy this solvent avoids the leaching of gold[15] and does not change the crystalline phase of the polymeric support, thus evidencing the role of the crystalline host polymer phase over the catalytic

Published as J. Catal. 2016, 340, 30-40. doi.org/10.1016/j.jcat.2016.05.005

performances of the AuNPs. The **Au-Cδ** catalyst afforded the quantitative conversion of NB into aniline (**AN**) in 60 min (entry **1** of Table 1 and Figure 4a), yielding a turnover frequency (TOF) value of 690 h^{-1}, calculated considering the amount of AN produced in 10 min; **Au-Cε** showed the highest catalytic activity leading to the quantitative and selective formation of AN in 45 min (entry **4** of Table 1 and Figure 4d) and a TOF at 10 min of reaction of 1230 h^{-1}. To the best of our knowledge, the latter is among the highest value reported for gold catalysts when $NaBH_4$ is the reductant.[9,11,26-28] On the contrary, the **Au-Cβ** and **Au-Cγ** catalysts (entry **2** and **3** of Table 1) did not produce significant conversion into AN, even when the reaction time is prolonged to 24 h: azoxybenzene (AOB) and azobenzene (AB) are in this case the first and prevalent reaction products of the cascade of reduction reactions (see Figures 4b-c). Interestingly, the reaction of NB with $NaBH_4$ in the absence of the gold catalyst gave, under the same reaction conditions (Figure S4), the same results of **Au-Cβ** and **Au-Cγ** suggesting that the first reaction steps, leading to AOB and AB, readily occur in methanol without involving the gold catalyst.

Table 1. Reduction of NB catalyzed by **Au-Cδ**, **Au-Cβ**, **Au-Cγ**, **Au-Cε** at 35 °C.

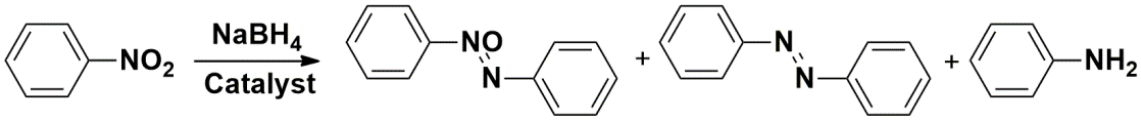

Entry[a]	Catalyst	Time (*min*)	Conversion[b] (*mol*%)	Selectivity[b] (%)		
				AOB	AB	AN
1	**Au-Cδ**	60	>99	-	-	>99
2	**Au-Cβ**	60	85	66	16	2.9
3	**Au-Cγ**	60	66	55	6.9	2.5
4	**Au-Cε**	45	>99	-	-	>99
5	-	90	86	67	14	5

[a] Reaction conditions: NB (2.54 mmol; 0.42M), gold catalyst (50 mg; NB/Au molar ratio = 500); $NaBH_4$ (15.2 mmol; 2.53 M), 35 °C, methanol (6 mL), N_2 protective atmosphere (1 bar). [b] Conversion and selectivity evaluated by GC-MS using anisole as internal standard.

Published as J. Catal. 2016, 340, 30-40. doi.org/10.1016/j.jcat.2016.05.005

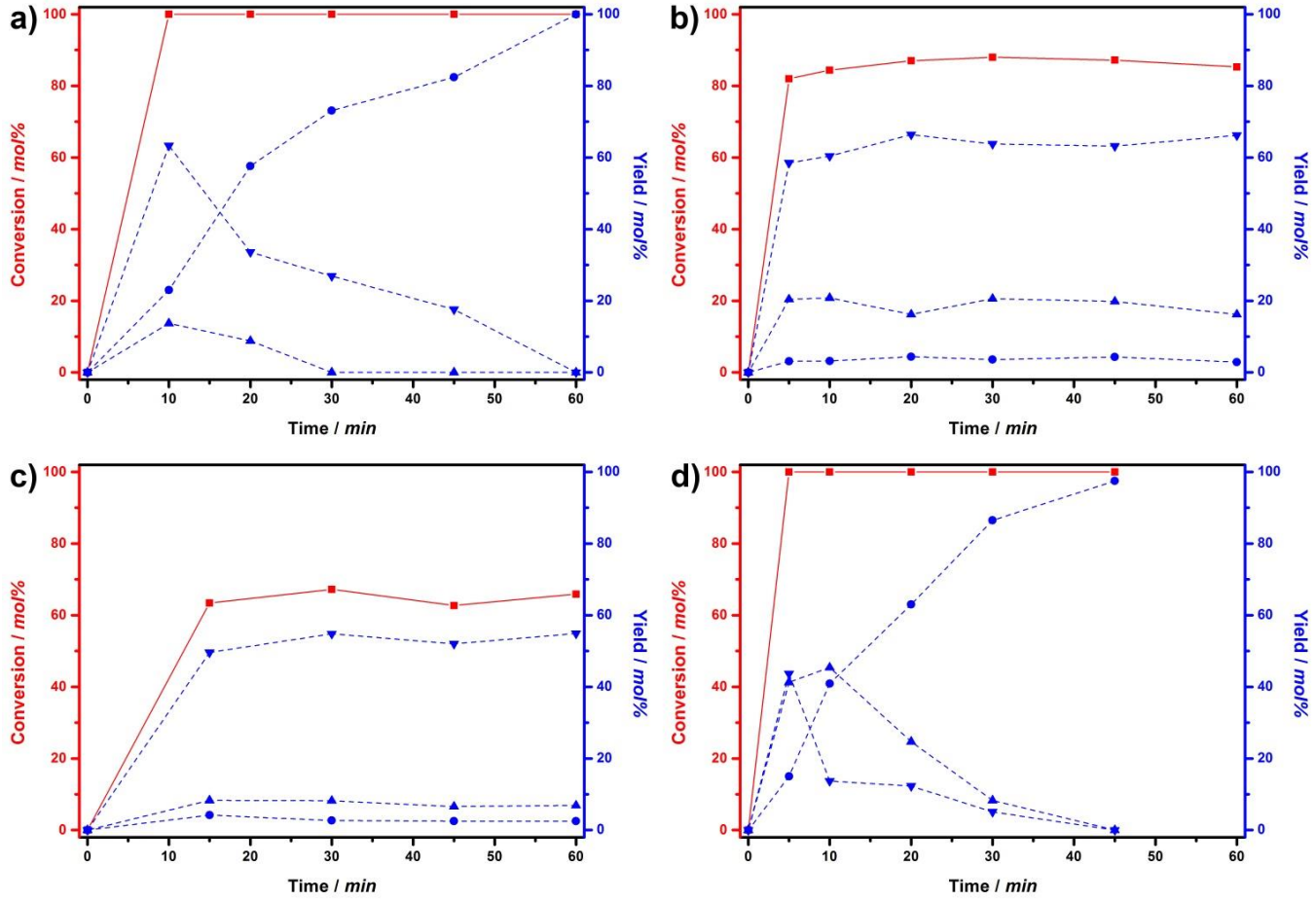

Figure 4. Reaction profiles for the NB reduction catalyzed by: a) **Au-Cδ** (entry **1**, Table 1); b) **Au-Cβ** (entry **2**, Table 1); c) **Au-Cγ** (entry **3**, Table 1); d) **Au-Cε** (entry **4**, Table 1). (■ = NB conversion; ▼= AOB yield; ▲= AB yield; ● = AN).

The reaction profiles of Figure 4 provide further mechanistic details on the course of the NB reduction at 35°C. The NB conversion catalyzed by **Au-Cδ** and **Au-Cε** is quantitative in few minutes leading to AOB and AB as reaction intermediates; the concentration of these compounds rapidly and quantitatively decreases in favor of the expected secondary reaction product AN, whose concentration steadily increases over reaction time (entry **1** and **4** of Table 1; Figures 4a and 4d).

The reaction temperature was varied in order to understand the evolution of the reaction intermediates. AOB and AB were accumulated at the initial stage of the reaction at 25°C (entry **1** of Table 2 and Figure 5a), whereas at 45°C and 55°C the **Au-Cε** catalyst produces faster conversion of both the intermediates into AN. The reaction is complete in 45 min at 45 °C, and in only 30 min at 55 °C (entry **2** and **3** of Table 2; Figure 5 b and c). The TOF at 55 °C reached the remarkable value of 2310 h^{-1} (entry **3** of Table 2; Figure 5c).

Published as J. Catal. 2016, 340, 30-40. doi.org/10.1016/j.jcat.2016.05.005

Table 2. Reduction of NB catalyzed by **Au-Cε** under different experimental conditions.

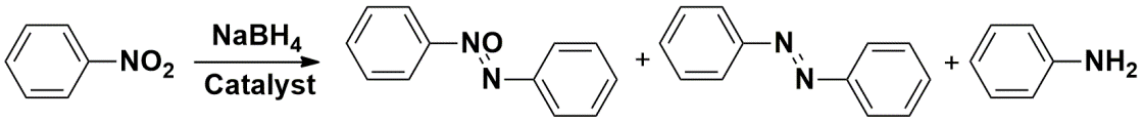

Entry[a]	T (°C)	$NaBH_4$/NB (*molar ratio*)	NB/Au (*molar ratio*)	Time (*min*)	Conversion[b] (*mol%*)	Selectivity[b] (*%*)		
						AOB	AB	AN
1	25	6	500	5	>99	66	20	14
				45	>99	13	4.0	83
				60	>99	-	-	>99
2	45	6	500	5	97	30	12	55
				20	97	22	-	75
				60	>99	-	-	99
3	55	6	500	30	>99	-	-	96
4	25	6	1000	5	97	80	14	2.0
				30	>99	24	59	17
				105	>99	-	-	>99
5[c]	25	6	2000	10	94	75	16	2.1
				120	>99	51	38	11
6	25	3	1000	5	92	74	14	3.7
				60	>99	44	29	27
				120	>99	50	15	35
7	25	12	1000	30	>99	80	16	2.4
				120	>99	29	60	11
				24 h	>99	-	-	>99
8	25	1	1000	10	79	73	5	1
				20	92	86	5	0.7
				30	92	89	3	0.4
9[d]	25	6	1000	45	>99	26	40	34
				105	>99	3.3	9.5	87
				120	>99	0.7	4.7	95

[a] Reaction conditions: NB (2.54 mmol, 0.42M), **Au-Cε**, methanol (6 mL), N_2 protective atmosphere (1 bar). [b] Conversions and selectivity determined by GC-MS analysis using anisole as internal standard. [c] NB = 5.08 mmol. [d] Reaction carried out in air.

Published as J. Catal. 2016, 340, 30-40. doi.org/10.1016/j.jcat.2016.05.005

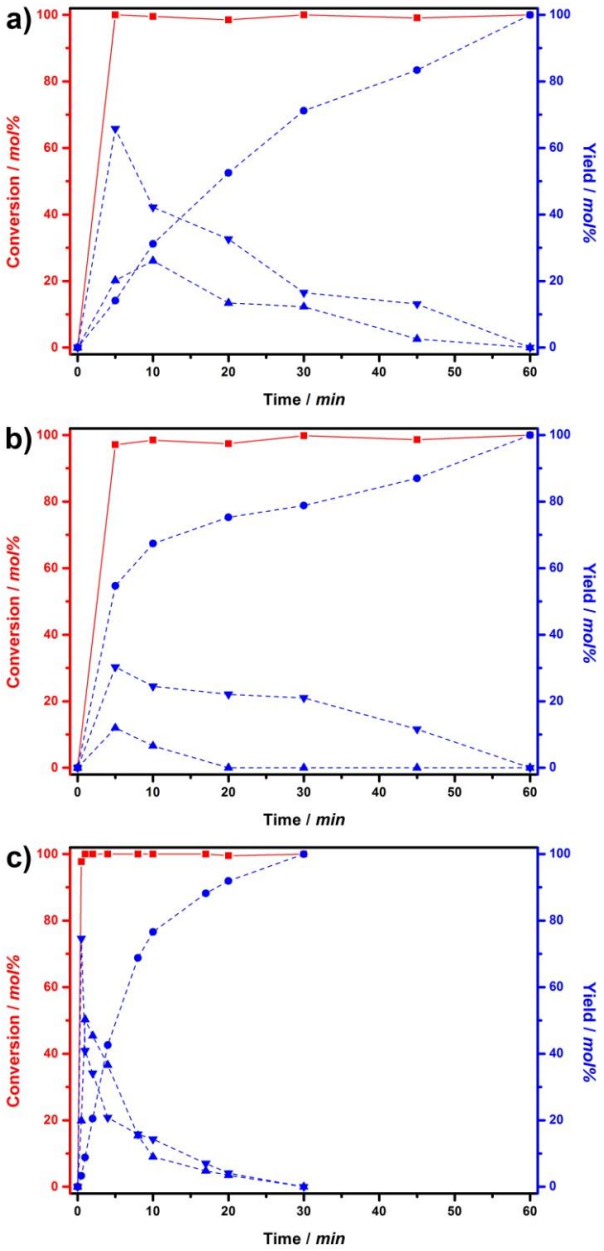

Figure 5. Effect of temperature in NB reduction: a) 25 °C (entry **1**, Table 2); b) 45°C (entry **2**, Table 2; c) 55°C (entry **3**, Table 2). (■ = NB conversion; ▼= AOB yield; ▲= AB yield; ● = AN yield).

At the NB/Au mole ratio of 1000, the full conversion of NB into AN was achieved in 105 min (entry **4** of Table 2; Figure S5), whereas a prolonged reaction time was necessary at the mole ratio of 2000 (entry **5** of Table 2; Figure S6).

Both the rate and selectivity of **Au-Cε** are strongly dependent on the $NaBH_4$ concentration. In the mild reaction condition of entry **4** of Table 2 the NB conversion into AN is quantitative in 105 min, at a $NaBH_4$/NB mole ratio of 6; decreasing this ratio to 3 or by increasing to 12 yields the partial reduction of NB into AB (compare entries **4**, **6** and **7** of Table 2 and Figure S5, S7 and S8). In the first case the $NaBH_4$ concentration is too low to allow the complete reduction into AN; at high

Published as J. Catal. 2016, 340, 30-40. doi.org/10.1016/j.jcat.2016.05.005

concentration both the hydride and the arene compete for the same catalytic sites and the reaction proceeds slowly as a result of a Langmuir-Hinshelwood mechanism[8b,27,29] (see also Figure S11). Interestingly a further decrease of $NaBH_4$ to 1 equiv. caused the exclusive formation of AOB in high yield (entry **8**, Table 2, Figure S9), that is an additional attractive synthetic target.[30]

In the head to head comparison of the NB reduction reaction catalyzed by **Au-Cε** in N_2 atmosphere and air, the yields in AN are the same whereas AB is only a minor product (compare entry **4** and **9** of Table 2 and Figure S5 with S10); this finding rules out that the aerobic oxidation of AN could lead to AB in high yields[31] under our experimental conditions.

Methanol is the best solvent, determining the highest activity and selectivity in AN (Figure **6**). In ethanol the AN yield is of 18 % in 2 h at 25 °C, whereas AOB and AB are the main reaction products, in 27 and 55 % yields, respectively (entry **S1** of Table S8 and Figure S12). Considering the hydrophobic nature of the host polymer matrix, water could be expected to be not an optimal solvent, as actually found (see Figure 6, entry **S5** of Table S8 and Figure S16): the conversion into AN is low since the diffusion of the reagents towards the catalytic site is hampered by the inefficient polymer swelling. AOB is the main product when the reaction is carried out in ethylene glycol, 1-propanol and 1-butanol (see entries **S2-4** of Table S8 and Figures S13-15) as a result of the slow diffusion of the reagents in these solvents through the cavity and channels of the nanoporous host polymer matrix.[16]

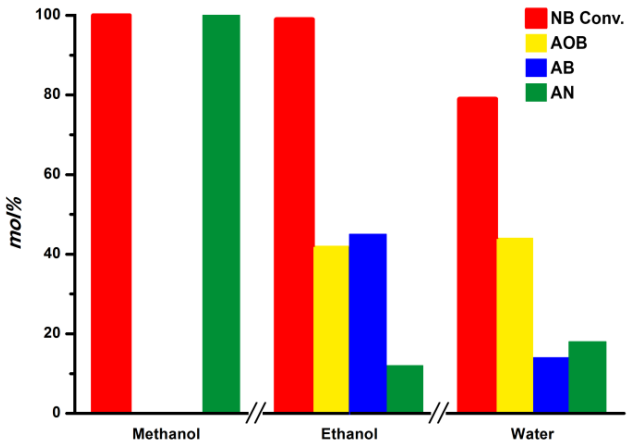

Figure 6. Selectivity of the NB reduction catalyzed by **Au-Cε** in methanol, ethanol and water (Table S15). [Reaction condition: NB (2.54 mmol, 0.42M), **Au-Cε** (25 mg, NB/Au molar ratio = 1000), $NaBH_4$ (15.2 mmol), 25°C, solvent (6 mL), N_2 protective atmosphere (1 bar), reaction time of 105 min.]

The inspection of the reaction profiles in Figure 4 and Figure 5 suggests that both AOB and AB are prevailingly formed in methanol solution and their diffusion, through the porous polymer matrix, is the rate determining step for the formation of AN at the gold catalytic sites. The plot of the mole concentration of AN *vs* reaction time, analyzed when the mole concentration of the intermediate species reached a negligible value, provided the apparent rate constant of $1.21 \cdot 10^{-4} \pm 1.6 \cdot 10^{-5}$ mol L^{-}

Published as J. Catal. 2016, 340, 30-40. doi.org/10.1016/j.jcat.2016.05.005

^{1} s^{-1} (25°C), $1.92\cdot10^{-4}\pm2.4\cdot10^{-5}$ mol L^{-1} s^{-1} (35°C) and $5.55\cdot10^{-4}\pm4.0\cdot10^{-5}$ mol L^{-1} s^{-1} (55°C); the corresponding Arrhenius plot gave an activation energy of 42±3 kJ mol^{-1} (see Figure S25) that well compares with those reported for the reduction of 4-nitrophenol (21-55 kJ mol^{-1}).[8e,27,29,32]

Table 3. Reduction of substituted nitroarenes catalyzed by **Au-Cε**.

Entry[a]	Substrate	Time (*h*)	Conversion[b] (*mol%*)	Products	Selectivity[b] (*%*)
1[c]	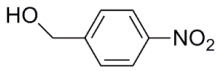 4-nitrobenzyl alcohol	1.5	>99	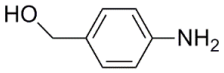 4-aminobenzyl alcohol	>99
2[c]	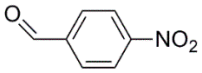 4-nitrobenzaldehyde	2	>99	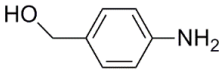 4-aminobenzyl alcohol	>99
3	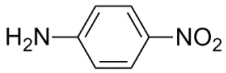 4-nitroaniline	6	>99	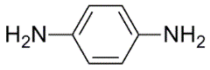 1,4-diaminobenzene	>99
4	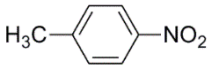 4-nitrotoluene	6	>99	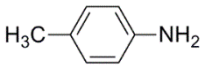 4-toluidine	98
5	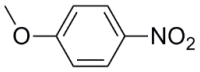 4-nitroanisole	6	>99	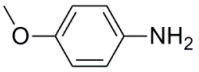 4-anisidine	91
6	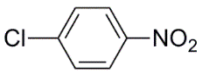 4-chloronitrobenzene	24	>99	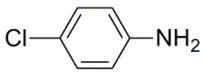 4-chloroaniline	93

[a] Reaction conditions: nitroarene (2.54 mmol), **Au-Cε** (Au loading = 0.1 *mol*%), 35 °C, $NaBH_4$/NB molar ratio of 6, methanol (6 mL), N_2 protective atmosphere (1 bar). [b] Conversion and selectivity evaluated by ^{1}H NMR analysis. [c] Reaction carried out at 25°C.

To further expand the scope of this study the catalytic performance of **Au-Cε** in the reduction of a variety of *p*-substituted nitroarenes was screened under the conditions of Table 3. The reduction of 4-nitrobenzyl alcohol and 4-nitrobenzaldehyde yields 4-aminobenzyl alcohol in 1.5h and 2h, respectively (entries **1** and **2** of Table 3)[8e,f] whereas *p*-amino-, *p*-methyl- and *p*-methoxy- substituted nitroarenes afforded the corresponding anilines with high selectivity in 6h (entries **3**, **4** and **5** of Table 3). The reduction of *p*-chloro nitrobenzene (entry **6** of Table 3) needs longer reaction time (24 h) and affords the corresponding aniline in moderate selectivity. The interpretation of these data is not immediate since the reaction rate is affected by several factors, among which the diffusion of the reactant through the polymer matrix which in turn depends on both the polarity and the steric bulkiness of the guest molecule.[33]

Published as J. Catal. 2016, 340, 30-40. doi.org/10.1016/j.jcat.2016.05.005

Finally, the **Au-Cε** catalyst was reused for four times under the reaction condition of entry **1** of Table 2 without observing loss of catalytic activity and selectivity (see Table S15 in the Supplementary Material).

Reaction mechanism. The reaction mechanism of NB reduction catalyzed by noble metal nanoparticles is currently matter of discussion in the scientific literature.[8f,9,34] Haber first proposed in 1898 the multistep reduction pathway comprising the two main routes of Scheme 1a.[35] In the *"direct route"* nitrosobenzene and phenylhydroxylamine are the primary reduction products, in the order; the formation of these two intermediates proceeds faster than phenylhydroxylamine reduction into AN, that is the rate determining step. In the *"condensation route"*, the reaction of nitrosobenzene with phenylhydroxylamine rapidly yields AOB that is reduced into AB and finally into AN through the diphenylhydrazine intermediate. The course of the reaction depends on the experimental conditions, namely the metal catalyst, the temperature, the reductant and the nitroaromatic/reductant molar ratio. In two elegant papers Corma *et al*. demonstrated that NB reduction catalyzed by Au-TiO_2 in the presence of H_2 proceeds through the *direct route* involving the phenylhydroxylamine intermediate (Scheme 1b).[6b,36] The FTIR monitoring of the reaction showed that at low coverage degree of the AuNPs surface, nitrosobenzene is rapidly transformed into phenylhydroxylamine and then into AN; the latter reaction is commonly considered the rate determining step. At high nitrosobenzene coverage, using *e.g.* the nanoparticulate Au-CeO_2 catalyst, the accumulation of this compound leads to its fast condensation with phenylhydroxylamine, thus opening the way to the condensation route.

Our study confirms that both the reaction pathways, namely the direct and condensation routes, are possible in the presence of $NaBH_4$ but the condensation route is preferred under the conditions of Table 1 and 2 (Scheme 1c). Actually $NaBH_4$ rapidly reduces NB to both AOB and AB without involving the gold catalyst. The reaction profiles of Figure 4 show that the conversion of NB into AOB and AB is quantitative within 10 min, and this also occurs in both the blank reaction or in the presence of the not porous **Au-Cβ** and **Au-Cγ** catalysts. Their formation indirectly further proves that nitrosobenzene and phenylhydroxylamine are the first elusive intermediates in the cascade of reduction reactions. The accumulation of phenylhydroxylamine, which cannot be further reduced into AN in the absence of the gold catalyst, leads to AOB and AB that are rapidly and selectively reduced into AN by the porous **Au-Cδ** and **Au-Cε** catalysts. Noteworthy the rate constants and the activation energy found in the NB reduction reaction catalyzed by **Au-Cδ** and **Au-Cε** are in the range typically found for the most active gold catalysts.[9,11,26-28] On the contrary, when the gold surface is rapidly accessible to the reactants, as in the case of catalysts showing easy accessible gold nanoparticles, the direct route is preferred. The lack of direct evidences for the presence of nitrosobenzene in the reaction media prompted some authors to propose the direct reduction of NB to phenylhydroxylamine excluding the nitrosobenzene intermediacy. Our results suggest that this is due simply to the fast reduction of phenylhydroxylamine into AN that hampers the condensation route.

There is a general consensus that a Langmuir–Hinshelwood mechanism is operative in this reaction; the coordination of the hydride species to the gold surface competes with that of the nitroaromatic

Published as J. Catal. 2016, 340, 30-40. doi.org/10.1016/j.jcat.2016.05.005

compounds to the same catalytic site.[32] We and others actually found that the increase of $NaBH_4$ concentration produces a decrease of NB conversion into AN (see Figure S18).

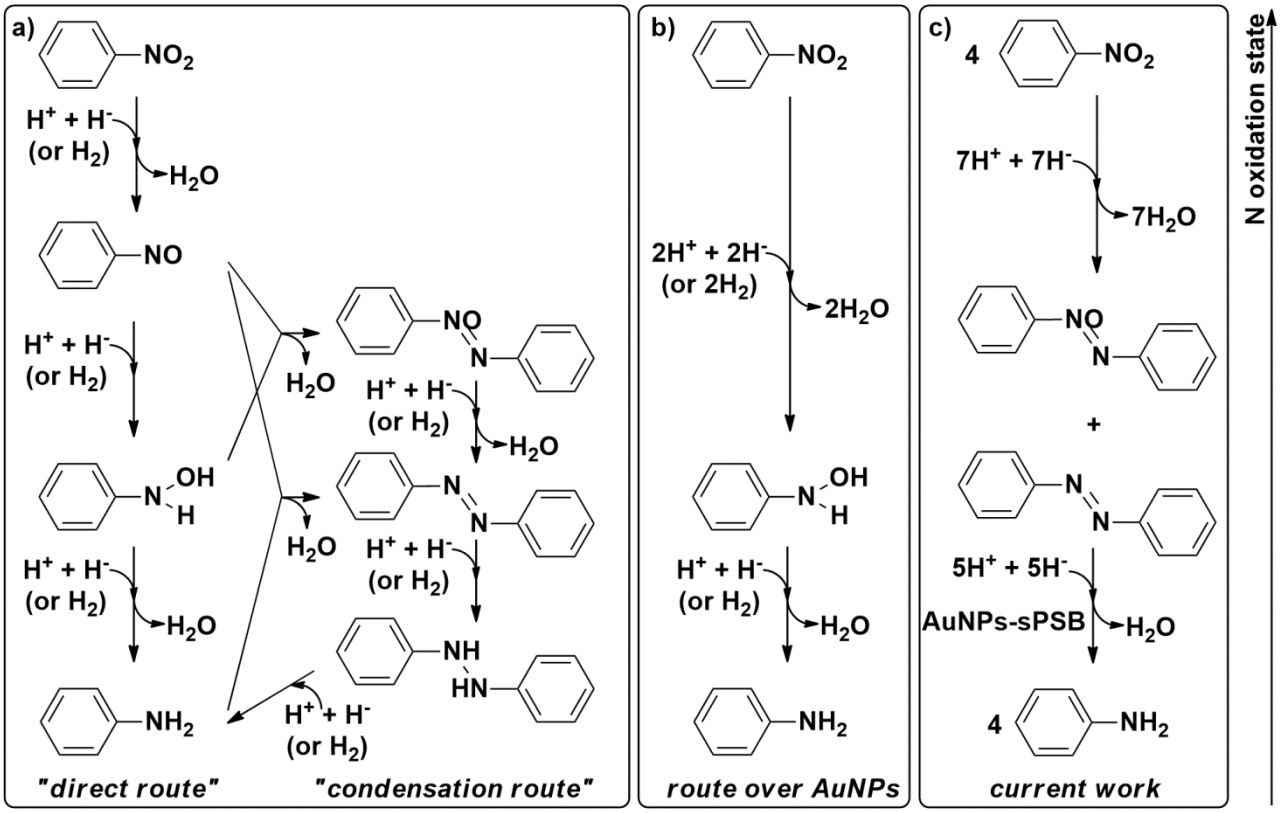

Scheme 1. a) Reaction mechanism for noble metal catalyzed NB reduction proposed by Haber; b) reaction pathway proposed for AuNPs with H_2 or $NaBH_4$ as reducing agent; c) reaction pathway identified in the current work.

4. CONCLUSION

The AuNPs-sPSB catalyst has been synthesized in four different crystalline phases of the polymer matrix, namely **Au-Cβ**, **Au-Cγ, Au-Cδ** and **Au-Cε**, to assess the role of the polymeric support on the conversion and selectivity in NB reduction when using $NaBH_4$ as reductant. The **Au-Cβ** and **Au-Cγ** catalysts show low specific surface area and porosity, as expected from the packing of the polymer chains in the crystalline phases, whereas **Au-Cδ** and **Au-Cε** exhibit specific surface area values of 16 and 24 m^2/g corresponding to the presence of nanovoids and nanochannels in the crystalline phase which can host both NB and the aromatic reaction intermediates. The catalytic runs promoted by **Au-Cβ**, **Au-Cγ, Au-Cδ** and **Au-Cε** were performed in methanol to avoid modification of the crystalline form of the polymer matrix in the course of the reaction. **Au-Cδ** and **Au-Cε** produce AN with TOF values in the range of the most active gold catalysts whereas **Au-Cβ** and **Au-Cγ** yielded AOB and AB as main reduction products: noteworthy these results are the same of the blank runs performed in the absence of the gold catalyst. The reaction profiles show that the formation of AOB and AB is fast, also outside of the polymer phase, and their diffusion through the

Published as J. Catal. 2016, 340, 30-40. doi.org/10.1016/j.jcat.2016.05.005

polymeric support allows the definitive reduction into AN. Previous studies demonstrated the prevalence of the *direct route* of the Haber mechanism when the gold catalyst is immediately accessible to the reactants, leading to the reduction of arylhydroxylamine into AN. On the contrary, the accumulation of the primary reaction intermediates, nitrosobenzene and arylhydroxylamine, promotes the condensation route that produces in many cases the partial reduction of NB into AOB and AB. The results herein reported show that: *i)* $NaBH_4$ can diffuse through the porous hydrophobic polymer matrix of sPSB in methanol, producing the Au-H species; *ii)* NB reduction into AOB and AB occurs, at least under the condition of this study, also in the absence of the gold catalyst; *iii)* both the intermediate reaction products, AOB and AB, rapidly diffuse through the polymer matrix of **Au-Cδ** and **Au-Cε** and are converted into AN with high activity and selectivity; *iv)* NB reduction is efficiently catalyzed by supported AuNPs in the presence of $NaBH_4$ through both the reaction routes proposed in the Haber mechanism, namely the direct and condensation routes: the latter is favored when the primary reduction products, nitrosobenzene and arylhydroxylamine, are not readily reduced by the gold catalyst.

APPENDIX A. SUPPLEMENTARY MATERIAL

Further details of BET analysis and reaction profiles.

ACKNOWLEDGMENTS

Financial support is acknowledged from the Ministero dell'Istruzione dell'Università e della Ricerca (MIUR, Roma, Italy for FARB 2014) and the SPRING cluster (REBIOCHEM research project CTN01_00063_49393). The Centro di Tecnologie Integrate per la Salute (Project PONa3_00138) for the 600 MHz NMR instrumental time is also acknowledged. The authors are also grateful to Dr. Patrizia Oliva, Dr. Patrizia Iannece and Mariagrazia Napoli from University of Salerno for technical assistance.

ABBREVIATIONS

AAS, atomic absorption spectroscopy; **AB**, azobenzene; **AN**, aniline; **AOB**, azoxybenzene; **AuNPs**, gold nanoparticles; **BET**, Brunauer-Emmet-Teller method; **ICP-OES**, inductively coupled plasma optical emission spectrometry; **NB**, nitrobenzene; **SEM**, scanning electron microscopy; **sPSB**, syndiotactic polystyrene-*co*-*cis*-1,4-polybutadiene multiblock copolymer; **SAED**, selected area electron diffraction; **TEM**, transmission electron microscopy; **WAXD**, powder wide angle x-ray diffraction;

REFERENCES

[1] *a*) M. Haruta, T. Kobayashi, H. Sano, N. Yamada, Chem. Lett., 16 (1987) 405-408; *b*) H. Tsunoyama, H. Sakurai, Y. Negishi, T. Tsukuda, J. Am. Chem. Soc., 127 (2005) 9374-9375; c) C.

Burato, P. Centomo, G. Pace, M. Favaro, L. Prati, B. Corain, J. Mol. Catal. A: Chem., 238 (2005) 26-34; *d*) H. Miyamura, R. Matsubara, Y. Miyazaki, S. Kobayashi, Angew. Chem. Int. Ed., 46 (2007) 4151-4154; *e*) L. Kesavan, R. Tiruvalam, M.H.A. Rahim, M.I. bin Saiman, D.I. Enache, R.L. Jenkins, N. Dimitratos, J.A. Lopez-Sanchez, S.H. Taylor, D.W. Knight, C.J. Kiely, G.J. Hutchings, Science, 331 (2011) 195-199; *f*) S.E. Davis, M.S. Ide, R.J. Davis, Green Chem., 15 (2013) 17-45; *g*) C.P. Vinod, K. Wilson, A.F. Lee, J. Chem. Technol. Biotechnol., 86 (2011) 161-171; *h*) T. Mallat, A. Baiker, Annu. Rev. Chem. Biomol. Eng., 3 (2012) 11-28; *i*) C. Lucchesi, T. Inasaki, H. Miyamura, R. Matsubara, S. Kobayashi, Adv. Synth. Catal., 350 (2008) 1996-2000; *l*) J. Huang, T. Akita, J. Faye, T. Fujitani, T. Takei, M. Haruta, Angew. Chem. Int. Ed., 48 (2009) 7862-7866.

[2] *a*) A. Abad, A. Corma, H. García, Chem. Eur. J., 14 (2008) 212-222; *b*) M.S. Ide, R.J. Davis, Acc. Chem. Res., 47 (2014) 825-833; *c*) B. Xu, X. Liu, J. Haubrich, C.M. Friend, Nat Chem, 2 (2010) 61-65; *d*) A. Wittstock, V. Zielasek, J. Biener, C.M. Friend, M. Bäumer, Science, 327 (2010) 319-322; *e*) M. Conte, H. Miyamura, S. Kobayashi, V. Chechik, J. Am. Chem. Soc., 131 (2009) 7189-7196; *f*) B.N. Zope, D.D. Hibbitts, M. Neurock, R.J. Davis, Science, 330 (2010) 74-78.

[3] P. Fristrup, L.B. Johansen, C.H. Christensen, Catal. Lett., 120 (2007) 184-190.

[4] *a*) M. Boronat, A. Corma, F. Illas, J. Radilla, T. Ródenas, M.J. Sabater, J. Catal., 278 (2011) 50-58; *b*) C. Shang, Z.-P. Liu, J. Am. Chem. Soc., 133 (2011) 9938-9947.

[5] G.M. Mullen, L. Zhang, E.J. Evans, T. Yan, G. Henkelman, C.B. Mullins, J. Am. Chem. Soc., 136 (2014) 6489-6498.

[6] A. Corma, P. Serna, Science, 313 (2006) 332-334; b) A. Corma, P. Concepción, P. Serna, Angew. Chem. Int. Ed., 46 (2007) 7266-7269.

[7] E. Vasilikogiannaki, C. Gryparis, V. Kotzabasaki, I.N. Lykakis, M. Stratakis, Adv. Synth. Catal., 355 (2013) 907-911.

[8] *a*) I. Tamiolakis, S. Fountoulaki, N. Vordos, I.N. Lykakis, G.S. Armatas, J. Mater. Chem. A, 1 (2013) 14311-14319; *b*) K. Layek, M.L. Kantam, M. Shirai, D. Nishio-Hamane, T. Sasaki, H. Maheswaran, Green Chem., 14 (2012) 3164-3174; *c*) Q. Ge, J. Ran, L. Wu, T. Xu, J. Appl. Polym. Sci., 132 (2015) 41268; *d*) Q. An, M. Yu, Y. Zhang, W. Ma, J. Guo, C. Wang, J. Phys. Chem. C, 116 (2012) 22432-22440; *e* D. Shah, H. Kaur, J. Mol. Catal. A: Chem., 381 (2014) 70-76; *f*) S. Fountoulaki, V. Daikopoulou, P.L. Gkizis, I. Tamiolakis, G.S. Armatas, I.N. Lykakis, ACS Catal., 4 (2014) 3504-3511.

[9] X. Liu, S. Ye, H.-Q. Li, Y.-M. Liu, Y. Cao, K.-N. Fan, Catal. Sci. Technol., 3 (2013) 3200-3206.

[10] *a*) J. Tormo, D.S. Hays, G.C. Fu, J. Org. Chem., 63 (1998) 5296-5297; *b*) R.G. de Noronha, C.C. Romão, A.C. Fernandes, J. Org. Chem., 74 (2009) 6960-6964.

[11] L. He, L.-C. Wang, H. Sun, J. Ni, Y. Cao, H.-Y. He, K.-N. Fan, Angew. Chem. Int. Ed., 48 (2009) 9538-9541.

[12] H. Zhu, X. Ke, X. Yang, S. Sarina, H. Liu, Angew. Chem. Int. Ed., 49 (2010) 9657-9661.

[13] *a*) W. Pitsawong, J. P. Hoben, A.–F. Miller, J. Biolog. Chem., 289 (2014) 15203-15214. *b*) P. R. Race, A. L. Lovering, R. M. Green, A. Ossor, S. A. White, P. F. Searle, C. J. Wrighton, I. E. Hyde, J. Biolog. Chem., 280 (2005) 13256-13264.

[14] A. Méndez–Villa, Current Research, Technology and Education Topics in Applied Microbiology and Microbial Biotechnology., Badajoz, Spain, 2010, pp.1008–1019.

[15] A. Buonerba, C. Cuomo, S. Ortega Sánchez, P. Canton, A. Grassi, Chem. Eur. J., 18 (2012) 709-715.

[16] A. Buonerba, A. Noschese, A. Grassi, Chem. Eur. J., 20 (2014) 5478-5486.

[17] *a*) P. Sharma, J. Chem. Pharm. Res. 3 (2011) 403-423; *b*) N.-H. Nam, Y.-J. You, Y. Kim, D.-H. Hong, H.-M. Kim, B.Z. Ahn, Bioorg. Med. Chem. Lett., 11 (2001) 1173-1176; *c*) S. Kumar, P. Arya, C. Mukherjee, B.K. Singh, N. Singh, V.S. Parmar, A.K. Prasad, B. Ghosh, Biochemistry, 44 (2005) 15944-15952; *d*) C. Keresszegi, T. Bürgi, T. Mallat, A. Baiker, J. Catal., 211 (2002) 244-251; *e*) N. Dimitratos, A. Villa, D. Wang, F. Porta, D. Su, L. Prati, J. Catal., 244 (2006) 113-121; *f*) L.J. Durndell, C.M.A. Parlett, N.S. Hondow, K. Wilson, A.F. Lee, Nanoscale, 5 (2013) 5412-5419.

[18] *a*) G. Milano, G. Guerra, Prog. Mater Sci., 54 (2009) 68-88; *b*) E.B. Gowd, K. Tashiro, C. Prog. Polym. Sci., 34 (2009) 280-315; *c*) E.M. Woo, Y.S. Sun, C.P. Yang, Prog. Polym. Sci., 26 (2001) 945-983; *d*) P. Rizzo, C. D'Aniello, A. De Girolamo Del Mauro, G. Guerra, Macromolecules, 40 (2007) 9470-9474; *e*) G. Guerra, V.M. Vitagliano, C. De Rosa, V. Petraccone, P. Corradini, Macromolecules, 23 (1990) 1539-1544; *f*) P. Rizzo, A.R. Albunia, G. Guerra, Polymer, 46 (2005) 9549-9554; *g*) C. De Rosa, O. Ruiz de Ballesteros, M. Di Gennaro, F. Auriemma, Polymer, 44 (2003) 1861-1870.

[19] *a*) P. Rizzo, C. Daniel, A. De Girolamo Del Mauro, G. Guerra, Chem. Mater., 19 (2007) 3864-3866; *b*) G. Guerra, C. Daniel, P. Rizzo, O. Tarallo, J. Polym. Sci., Part B: Polym. Phys., 50 (2012) 305-322. *c*) C. Manfredi, M.A. Del Nobile, G. Mensitieri, G. Guerra, M. Rapacciuolo, J. Polym. Sci., Part B: Polym. Phys., 35 (1997) 133-140; *d*) D. Larobina, L. Sanguigno, V. Venditto, G. Guerra, G. Mensitieri, Polymer, 45 (2004) 429-436; *e*) G. Mensitieri, D. Larobina, G. Guerra, V. Venditto, M. Fermeglia, S. Pricl, J. Polym. Sci., Part B: Polym. Phys., 46 (2008) 8-15; *f*) V. Petraccone, O. Ruiz de Ballesteros, O. Tarallo, P. Rizzo, G. Guerra, Chem. Mater., 20 (2008) 3663-3668.

[20] *a*) O. Tarallo, M.M. Schiavone, V. Petraccone, C. Daniel, P. Rizzo, G. Guerra, Macromolecules, 43 (2010) 1455-1466; *b*) C. Daniel, C. Rufolo, F. Bobba, A. Scarfato, A.M. Cucolo, G. Guerra, J. Mater. Chem., 21 (2011) 19074-19079.

[21] A.R. Albunia, P. Rizzo, M. Coppola, M. De Pascale, G. Guerra, Polymer, 53 (2012) 2727-2735.

[22] *a*) A. Buonerba, V. Speranza, P. Canton, C. Capacchione, S. Milione, A. Grassi, RSC Adv., 4 (2014) 60158-60167; *b*) A. Buonerba, M. Fienga, S. Milione, C. Cuomo, A. Grassi, A. Proto, C. Capacchione, Macromolecules, 46 (2013) 8449-8457; *c*) A. Buonerba, C. Cuomo, V. Speranza, A.

Grassi, Macromolecules, 43 (2010) 367-374; *d*) C. Capacchione, A. De Roma, A. Buonerba, V. Speranza, S. Milione, A. Grassi, Macromol. Chem. Phys., 214 (2013) 1990-1997.

[23] *Metal Nanoclusters in Catalysis and Material Science: The Issue of Size Control*, Corain, B., Schmid, G., Toshima, N., Elsevier, Amsterdam, **2008**, pp. 131 –132.

[24] K. Morgan, A. Goguet, C. Hardacre, ACS Catal., 5 (2015) 3430-3445.

[25] K. S. W. Sing, Adv. Colloid Interface Sci. 76-77 (1998) 3-11.

[26] a) P. Serna, A. Corma, ACS Catal., 5 (2015) 7114-7121; b) H.K. Kadam, S.G. Tilve, RSC Adv., 5 (2015) 83391-83407.

[27] T. Aditya, A. Pal, T. Pal, Chem. Commun., 51 (2015) 9410-9431.

[28] S. Panigrahi, S. Basu, S. Praharaj, S. Pande, S. Jana, A. Pal, S.K. Ghosh, T. Pal, J. Phys. Chem. C, 111 (2007) 4596-4605.

[29] S. Wunder, Y. Lu, M. Albrecht, M. Ballauff, ACS Catal., 1 (2011) 908-916.

[30] *a*) M.N. Pahalagedara, L.R. Pahalagedara, J. He, R. Miao, B. Gottlieb, D. Rathnayake, S.L. Suib, J. Catal., 336 (2016) 41-48; *b*) S. Ghosh, S.S. Acharyya, T. Sasaki, R. Bal, Green Chem., 17 (2015) 1867-1876.

[31] *a*) A. Grirrane, A. Corma, H. García, Science, 322 (2008) 1661-1664; *b*) A. Grirrane, A. Corma, H. Garcia, Nat. Protocols, 11 (2010) 429-438.

[32] S. Wunder, F. Polzer, Y. Lu, Y. Mei, M. Ballauff, J. Phys. Chem. C, 114 (2010) 8814-8820.

[33] C. Daniel, N. Galdi, T. Montefusco, G. Guerra, Chem. Mater., 19 (2007) 3302-3308.

[34] E.A. Gelder, S.D. Jackson, C.M. Lok, Chem. Commun., (2005) 522-524.

[35] F.Z. Haber, Elektrochem. 4 (1898) 506.

[36] D. Combita, P. Concepción, A. Corma, J. Catal., 311 (2014) 339-349.

Published as J. Catal. 2016, 340, 30-40. doi.org/10.1016/j.jcat.2016.05.005

Highly Efficient and Selective Reduction of Nitroarenes into Anilines Catalyzed by Gold Nanoparticles Incarcerated in a Nanoporous Polymer Matrix: Role of the Polymeric Support and Insight into the Reaction Mechanism

*Annarita Noschese,[a†] Antonio Buonerba,[ab†] Patrizia Canton,[c] Stefano Milione,[ab] Carmine Capacchione[ab] and Alfonso Grassi[ab]**

[a] Dipartimento di Chimica e Biologia "Adolfo Zambelli", Università degli Studi di Salerno, via Giovanni Paolo II, 84084 Fisciano (SA), Italy.

[b] CIRCC, Interuniversity Consortium Chemical Reactivity and Catalysis, via Celso Ulpiani 27, 70126 (BA), Italy.

[c] Dipartimento di Scienze Molecolari e Nanosistemi, Università Ca' Foscari Venezia, Via Torino 155/B, 30170 Mestre (VE), Italy.

[†] These authors contributed equally.

* Corresponding author. E-mail: agrassi@unisa.it.

Published as J. Catal. 2016, 340, 30-40. doi.org/10.1016/j.jcat.2016.05.005

Table of Contents.

Published as J. Catal. 2016, 340, 30-40. doi.org/10.1016/j.jcat.2016.05.005

Published as J. Catal. 2016, 340, 30-40. doi.org/10.1016/j.jcat.2016.05.005

1. BET Analysis.

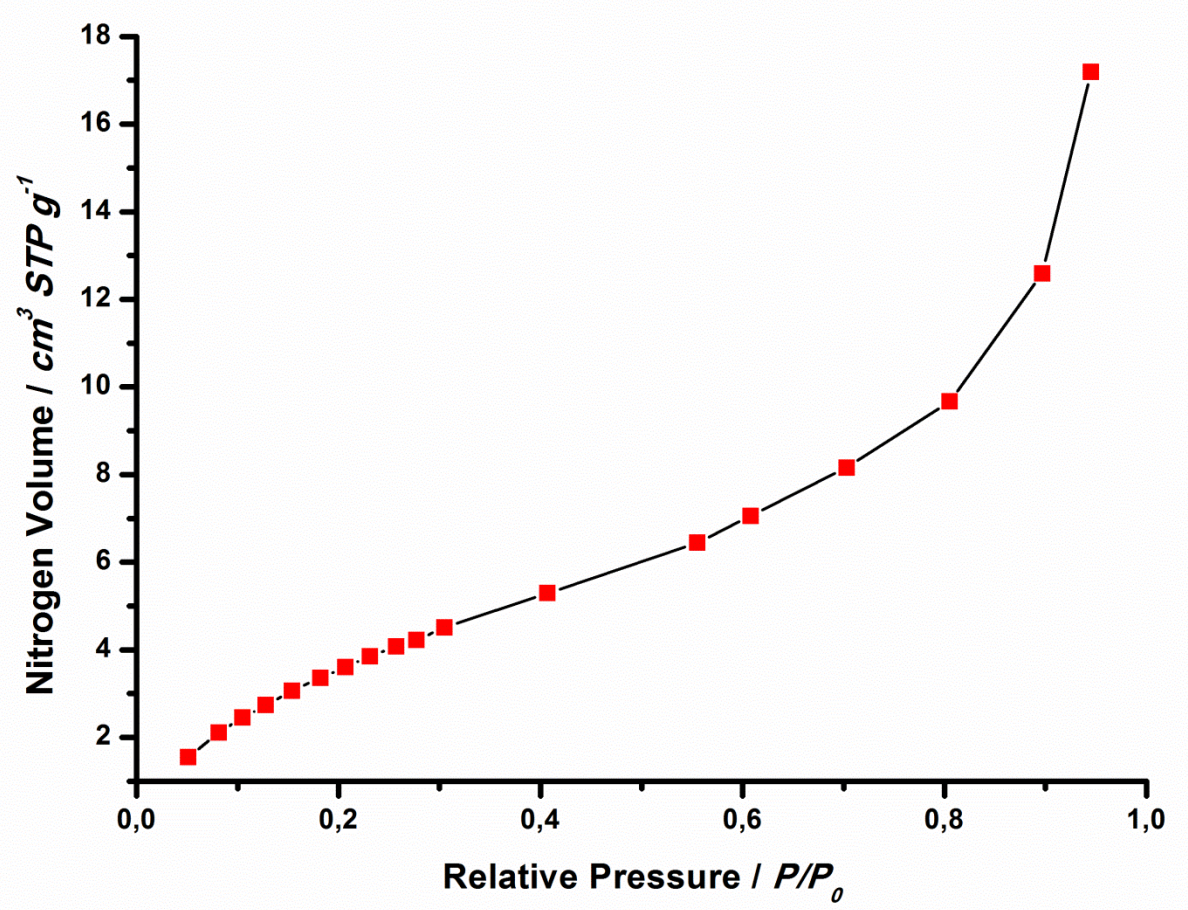

Figure S1. BET profile for the catalyst **Au-Cδ**.

Published as J. Catal. 2016, 340, 30-40. doi.org/10.1016/j.jcat.2016.05.005

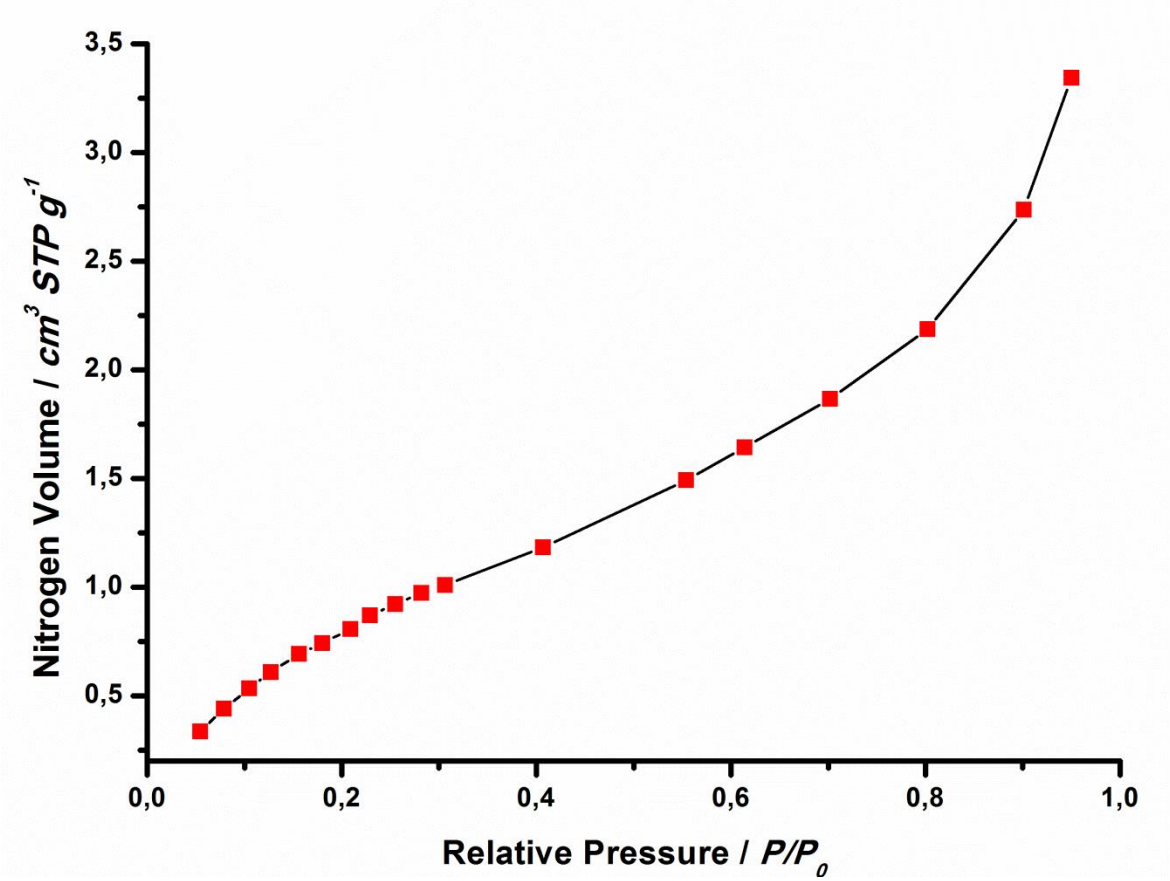

Figure S2. BET profile for the catalyst **Au-Cγ**.

Published as J. Catal. 2016, 340, 30-40. doi.org/10.1016/j.jcat.2016.05.005

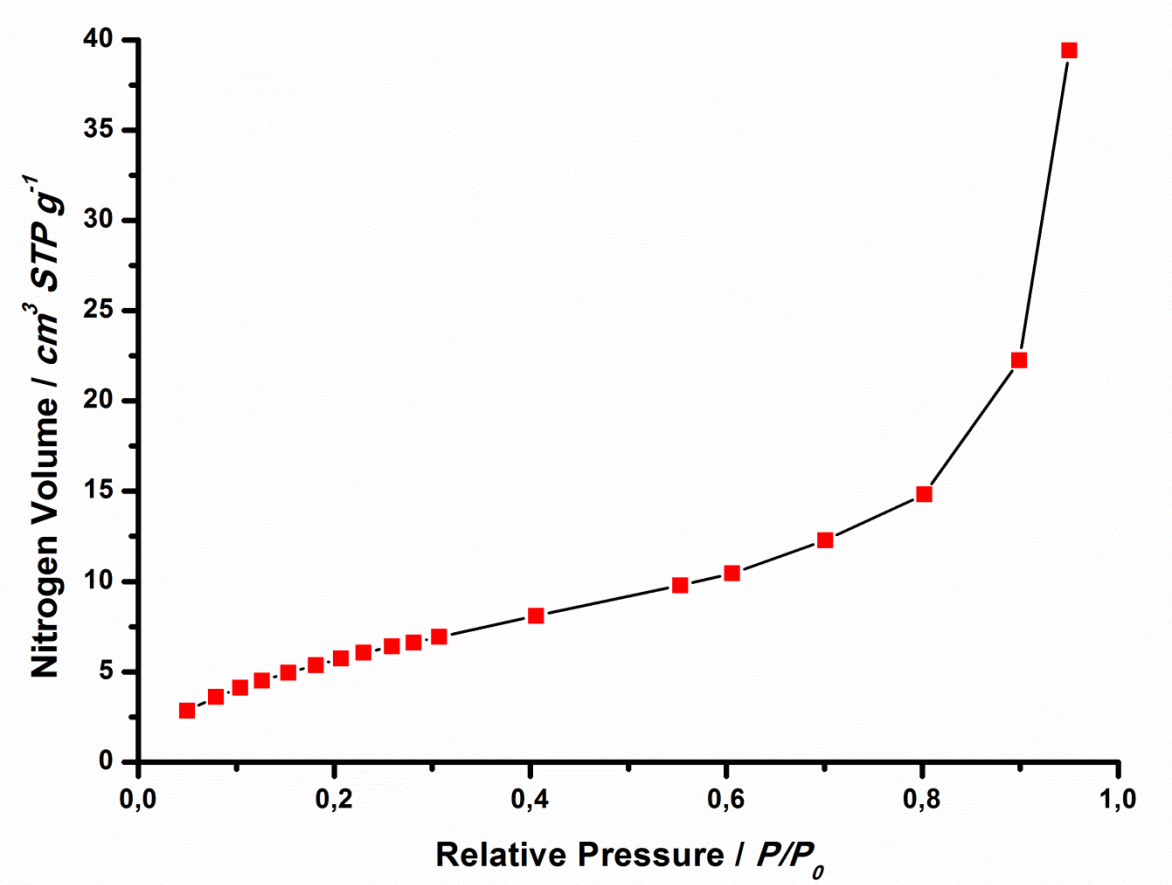

Figure S3. BET profile for the catalyst **Au-Cε**.

Published as J. Catal. 2016, 340, 30-40. doi.org/10.1016/j.jcat.2016.05.005

2. Reaction Profiles.

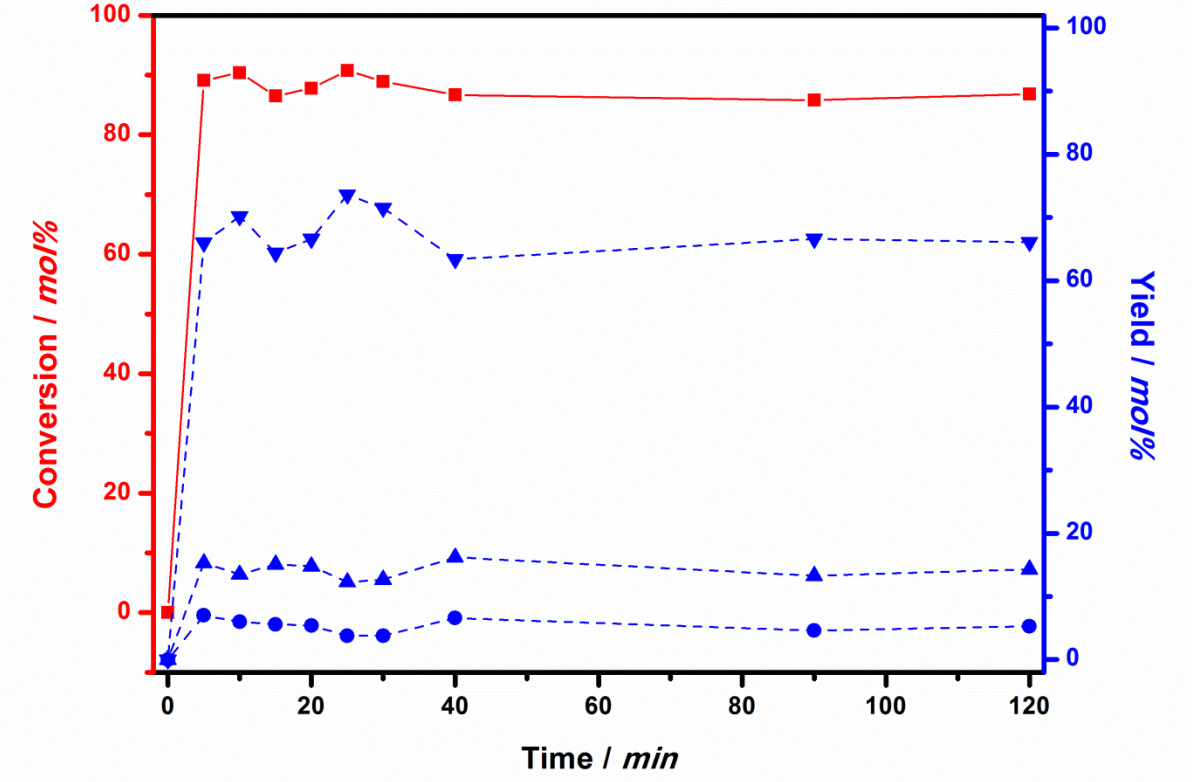

Figure S4. Reaction profile of entry **5** of Table 1.
(■ = NB conversion; ▼= AOB yield; ▲= AB yield; ● = AN yield).

Table S1. Course of the reaction of entry **5** of Table 1.

Time (*min*)	**NB Conversion (*mol%*)**	**Yield (*mol%*)**		
		AOB	**AB**	**AN**
5	89	66	15	7.0
10	90	70	14	6.0
15	86	64	15	5.6
20	88	67	15	5.4
25	91	74	12	3.8
30	89	72	13	3.8
40	87	63	16	6.6
90	86	67	13	4.6
120	87	66	14	5.3

Reaction Conditions: NB (2.54 mmol), $NaBH_4$ (15.2 mmol), MeOH (6 mL), 35 °C, N_2 atmosphere. Conversion and yields determined by GC-MS (anisole as internal standard).

Published as J. Catal. 2016, 340, 30-40. doi.org/10.1016/j.jcat.2016.05.005

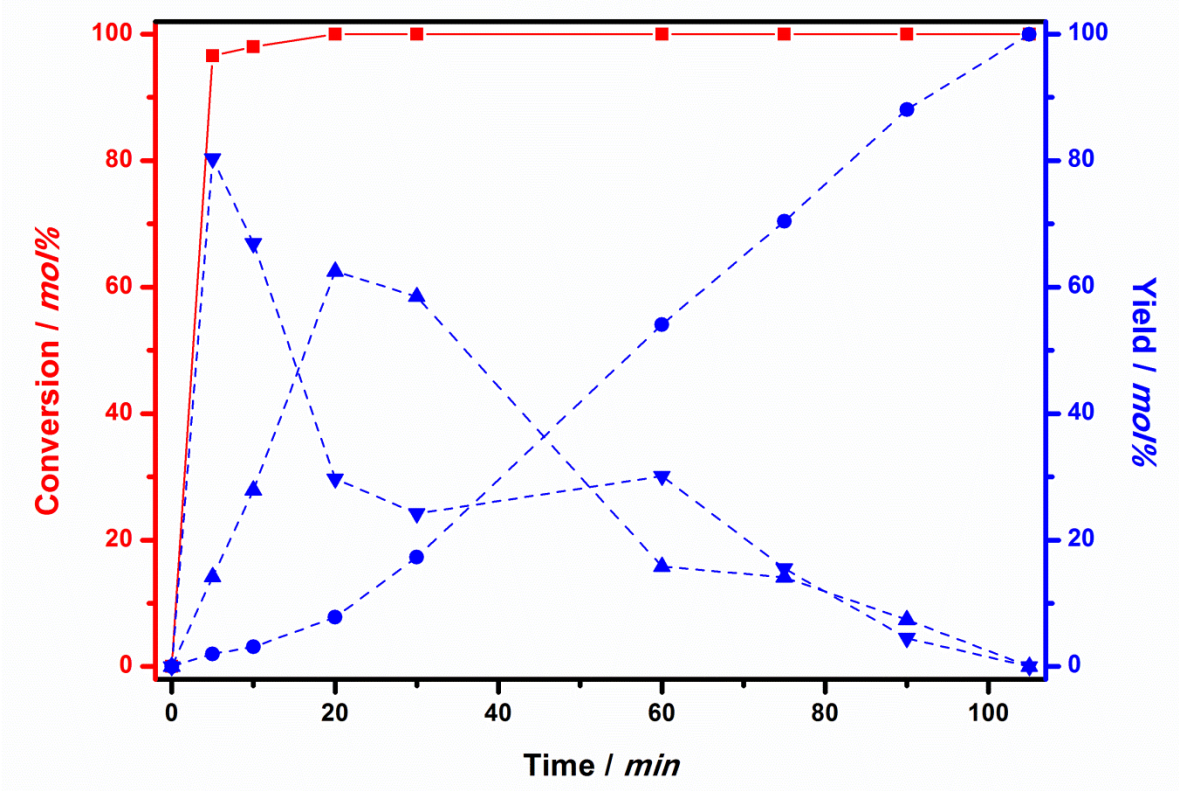

Figure S5. Reaction profile of entry **4** of Table 2.
(■ = NB conversion; ▼= AOB yield; ▲= AB yield; ● = AN yield).

Table S2. Course of the reaction of entry **4** of Table 2.

Time (*min*)	**NB Conversion (*mol%*)**	**Yield (*mol%*)**		
		AOB	**AB**	**AN**
5	97	80	14	2.0
10	98	67	28	3.0
20	>99	29	63	7.8
30	>99	24	59	17
60	>99	30	16	54
75	>99	16	14	70
90	>99	4.5	7.4	88
105	>99	0	0	>99

Reaction Conditions: NB (2.54 mmol), **Au-Cε** (50 mg; 0.1 *mol*% of Au), $NaBH_4$ (15.2 mmol), MeOH (6 mL), 25 °C, N_2 atmosphere. Conversion and yields determined by GC-MS (anisole as internal standard).

Published as J. Catal. 2016, 340, 30-40. doi.org/10.1016/j.jcat.2016.05.005

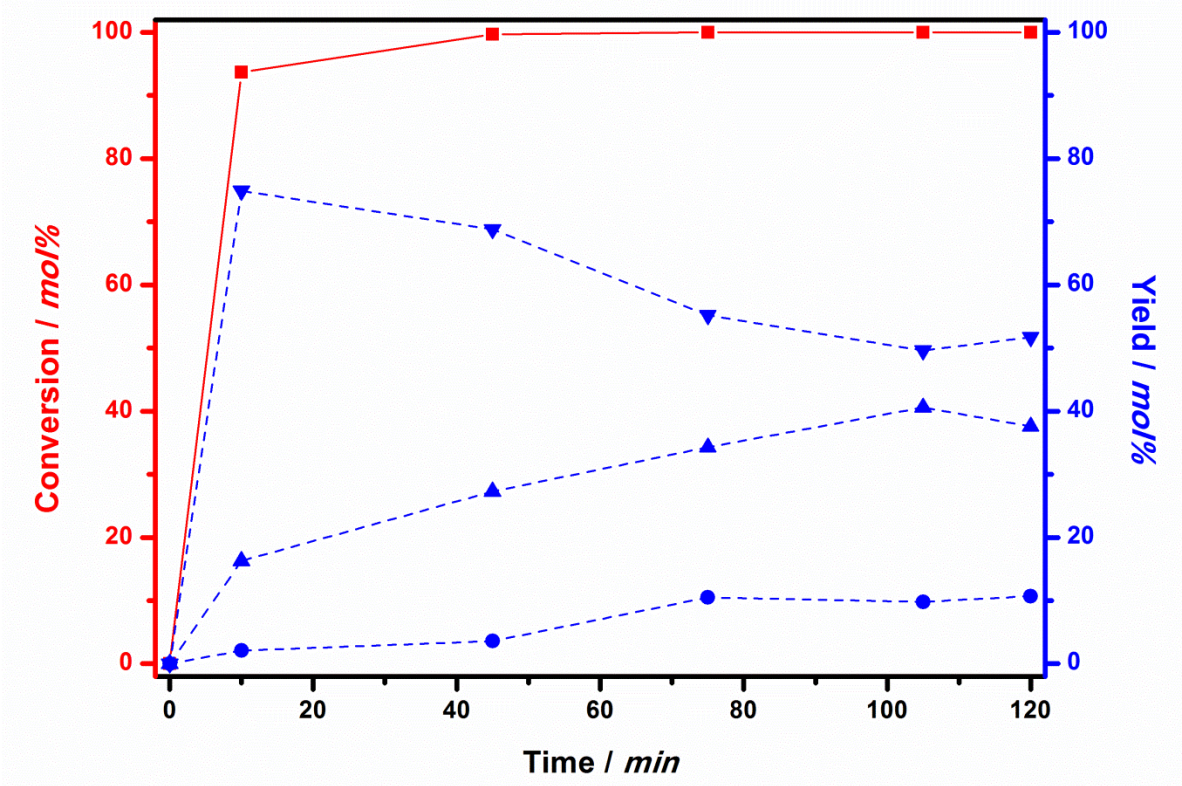

Figure S6. Reaction profile of entry **5** of Table 2.
(■ = NB conversion; ▼= AOB yield; ▲= AB yield; ● = AN yield).

Table S3. Course of the reaction of entry **5** of Table 2.

Time (*min*)	**NB Conversion (*mol%*)**	**Yield (*mol%*)**		
		AOB	**AB**	**AN**
10	94	75	16	2.1
45	>99	67	27	3.6
75	>99	55	34	11
105	>99	50	40	10
120	>99	51	38	11

Reaction Conditions: NB (5.08 mmol), **Au-Cε** (25 mg; 0.05 *mol*% of Au), $NaBH_4$ (30.5 mmol), MeOH (6 mL), 25 °C, N_2 atmosphere. Conversion and yields determined by GC-MS (anisole as internal standard).

Published as J. Catal. 2016, 340, 30-40. doi.org/10.1016/j.jcat.2016.05.005

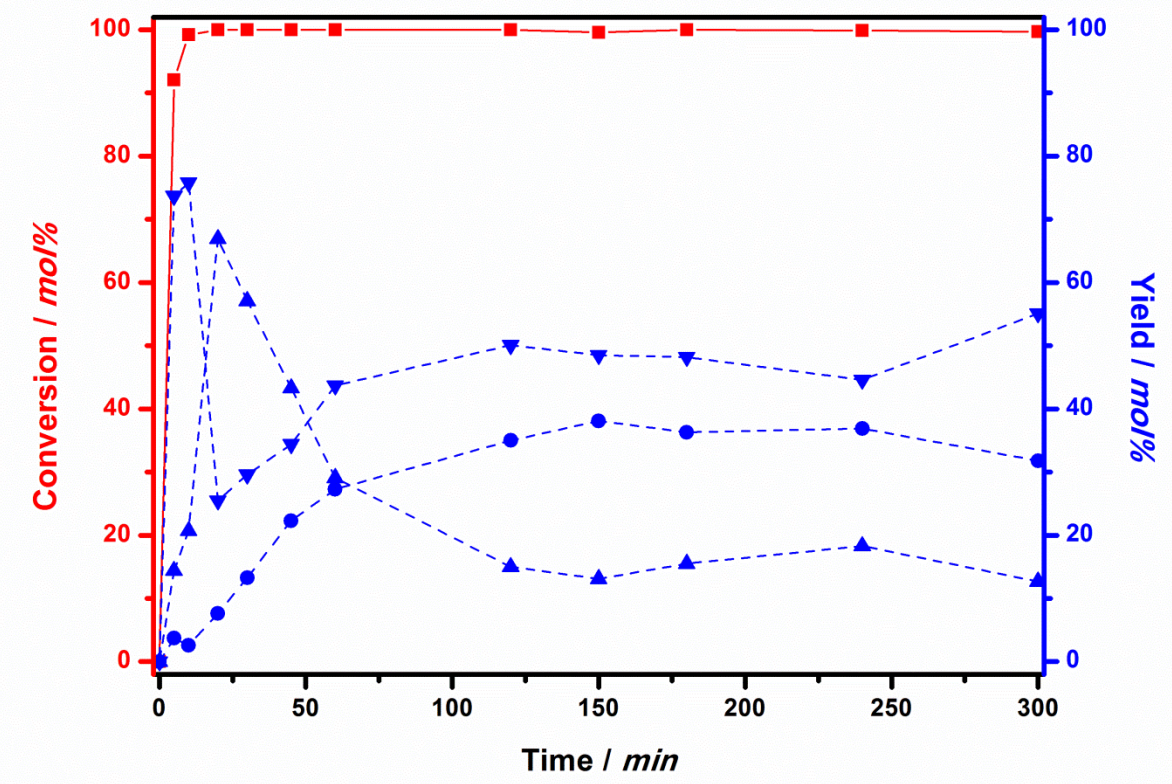

Figure S7. Reaction profile of entry **6** of Table 2.
(■ = NB conversion; ▼= AOB yield; ▲= AB yield; ● = AN yield).

Table S4. Course of the reaction of entry **6** of Table 2.

Time (*min*)	**NB Conversion (*mol%*)**	**Yield (*mol%*)**		
		AOB	**AB**	**AN**
5	92	74	14	3.7
10	99	76	21	2.6
20	>99	26	67	7.0
30	>99	30	57	13
45	>99	34	43	22
60	>99	44	29	27
120	>99	50	15	35
150	>99	49	13	38
180	>99	48	16	36
240	>99	45	18	37
300	>99	55	13	32

Reaction Conditions: NB (2.54 mmol), **Au-Cε** (25 mg; 0.1 *mol*% of Au), $NaBH_4$ (7.62 mmol), MeOH (6 mL), 25 °C, N_2 atmosphere. Conversion and yields determined by GC-MS (anisole as internal standard).

Published as J. Catal. 2016, 340, 30-40. doi.org/10.1016/j.jcat.2016.05.005

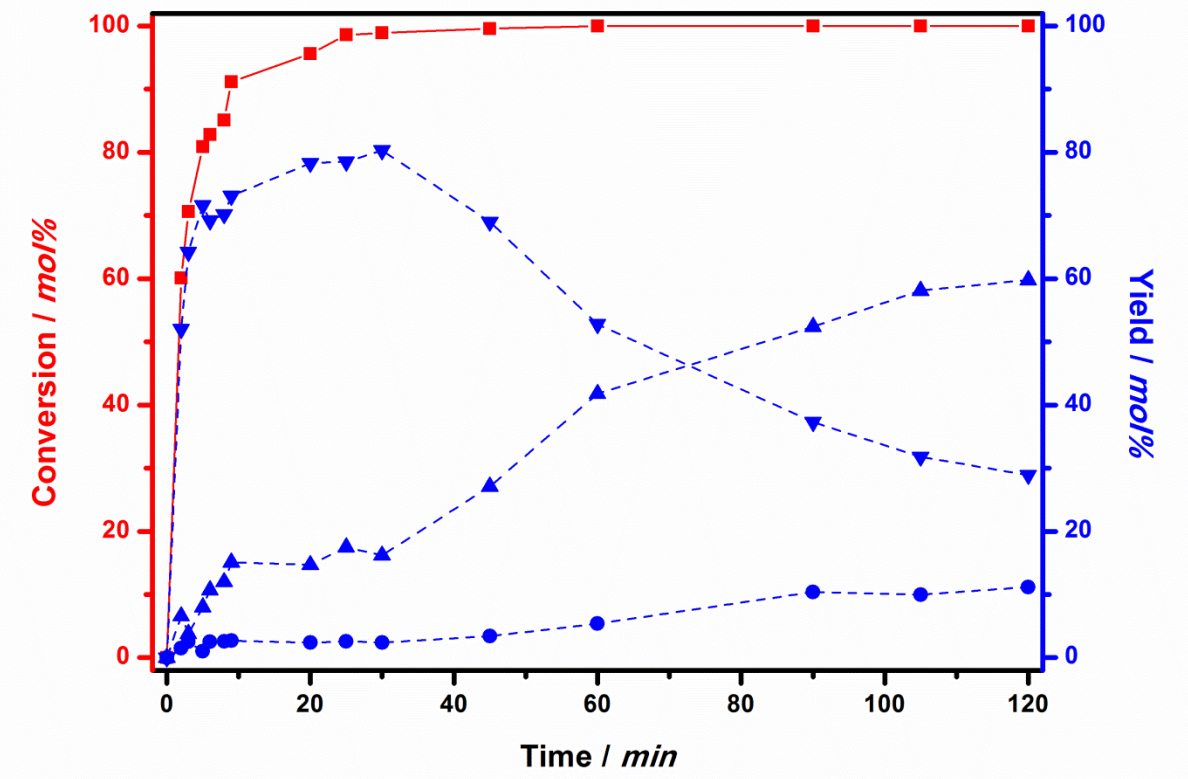

Figure S8. Reaction profile of entry **7** of Table 2.
(■ = NB conversion; ▼= AOB yield; ▲= AB yield; ● = AN yield).

Table S5. Course of the reaction of entry **7** of Table 2.

Time (*min*)	**NB Conversion (*mol%*)**	**Yield (*mol%*)**		
		AOB	**AB**	**AN**
2	60	52	6.5	1.5
3	71	64	3.8	2.5
5	81	72	8.0	1.0
6	83	69	11	2.5
8	85	70	12	2.6
9	91	73	15	2.7
20	96	78	15	2.4
25	99	79	17	2.6
30	99	80	16	2.4
45	>99	69	27	3.5
60	>99	53	42	5.0
90	>99	37	52	11
105	>99	31	57	12
120	>99	29	60	11

Reaction Conditions: NB (2.54 mmol), **Au-Cε** (25 mg; 0.1 *mol*% of Au), $NaBH_4$ (30.5 mmol), MeOH (6 mL), 25 °C, N_2 atmosphere. Conversion and yields determined by GC-MS (anisole as internal standard).

Published as J. Catal. 2016, 340, 30-40. doi.org/10.1016/j.jcat.2016.05.005

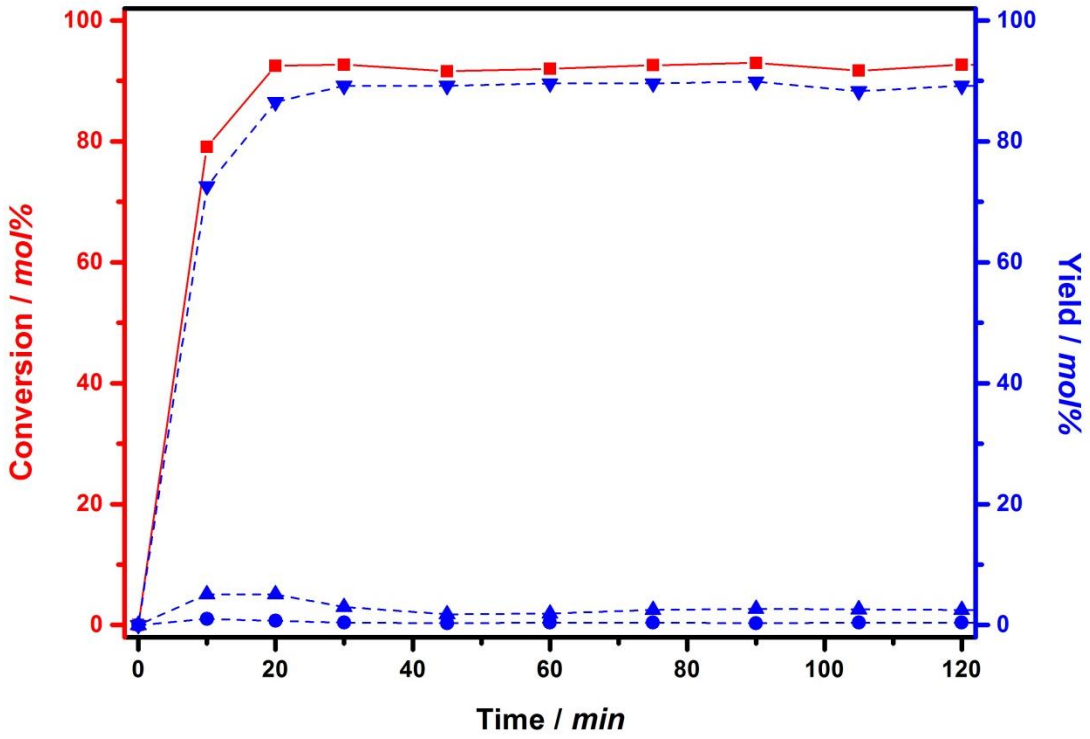

Figure S9. Reaction profile of entry **8** of Table 2.
(■ = NB conversion; ▼= AOB yield; ▲= AB yield; ● = AN yield).

Table S6. Course of the reaction of entry **8** of Table 2.

Time (*min*)	**NB Conversion (mole%)**	**Yield (*mol%*)**		
		AOB	**AB**	**AN**
10	79	72.6	5.1	1.0
20	92	86.5	5.1	0.7
30	92	89.2	3.0	0.4
45	92	89.2	1.8	0.3
60	92	89.6	1.9	0.4
75	92	89.6	2.5	0.4
90	93	89.9	2.7	0.3
105	92	88.3	2.6	0.4
120	93	89.2	2.5	0.4

Reaction Conditions: NB (2.54 mmol), **Au-Cε** (25 mg; 0.1 *mol*% of Au), $NaBH_4$ (2.54mmol), MeOH (6 mL), 25 °C, N_2 atmosphere. Conversion and yields determined by GC-MS (anisole as internal standard).

Published as J. Catal. 2016, 340, 30-40. doi.org/10.1016/j.jcat.2016.05.005

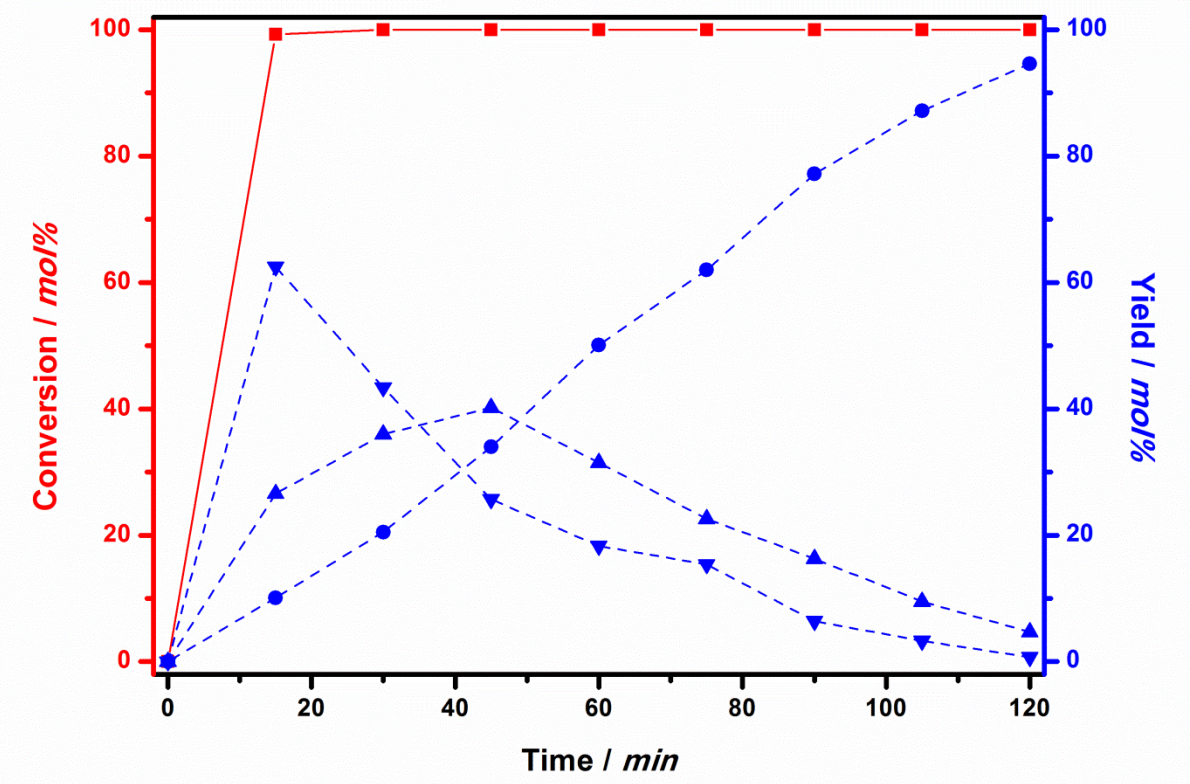

Figure S10. Reaction profile of entry **9** of Table 2.
(■ = NB conversion; ▼= AOB yield; ▲= AB yield; ● = AN yield).

Table S7. Course of the reaction of entry **9** of Table 2.

Time (*min*)	**NB Conversion (*mol%*)**	**Yield (*mol%*)**		
		AOB	**AB**	**AN**
15	99	63	27	10
30	>99	43	36	21
45	>99	26	40	34
60	>99	18	32	50
75	>99	15	23	62
90	>99	6.4	16	77
105	>99	3.3	9.5	87
120	>99	0.7	4.7	95

Reaction Conditions: NB (2.54 mmol), **Au-Cε** (25 mg; 0.1 *mol*% of Au), $NaBH_4$ (15.2mmol), MeOH (6 mL), 25 °C, reaction carried under air. Conversion and yields determined by GC-MS (anisole as internal standard).

Published as J. Catal. 2016, 340, 30-40. doi.org/10.1016/j.jcat.2016.05.005

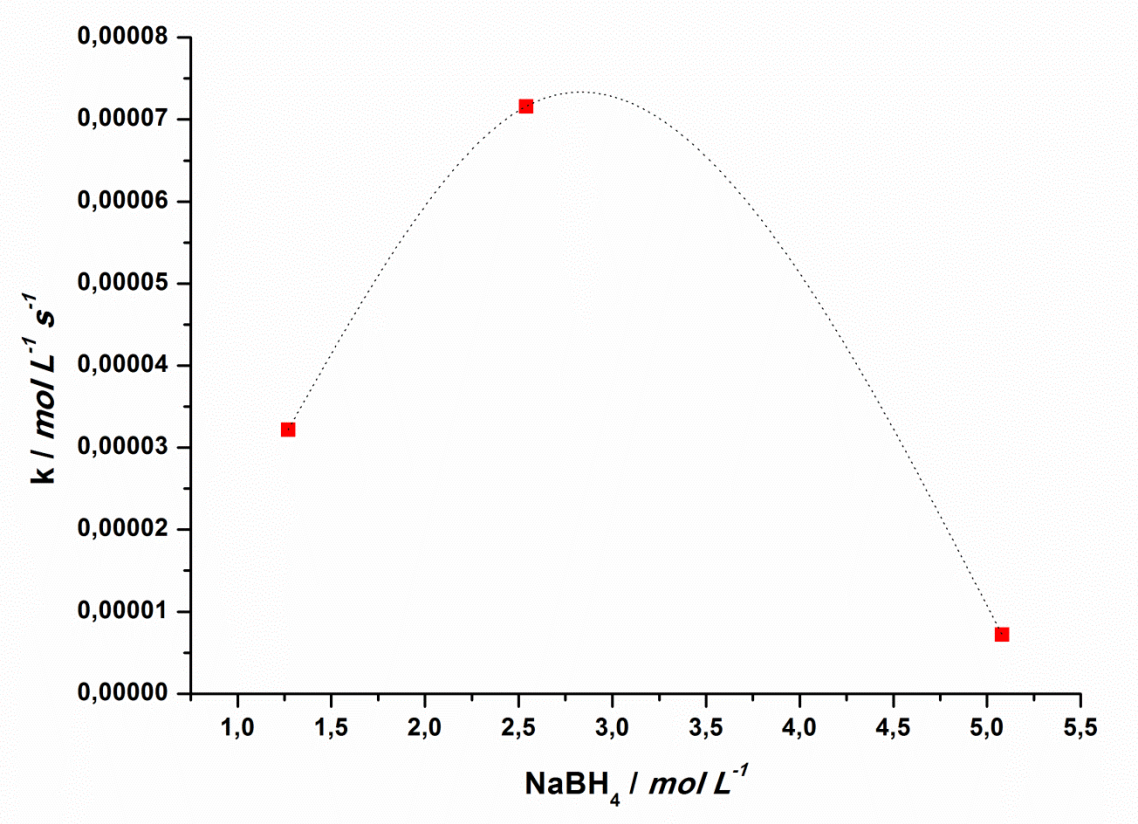

Figure S11. Trend of the apparent rate constant *k* (25°C; [NB] = 0.42 mol L^{-1}) at variance of the $NaBH_4$ concentration (1.3, 2.5 and 5.1 mol L^{-1}).

Published as J. Catal. 2016, 340, 30-40. doi.org/10.1016/j.jcat.2016.05.005

Table S8. Nitrobenzene reduction catalyzed by **Au-Cε** in different solvents.

Entry[a]	**Solvent**	**Time (*min*)**	**Conversion**[b] **(mole%)**	**Yield**[b] **(mole%)**		
				AOB	**AB**	**A**
S1	Ethanol	30	>99	54	41	4.8
		45	>99	52	42	5.8
		105	>99	42	45	13
		120	>99	27	55	18
S2	Ethylene glycol	20	66	39	7.0	18
		75	92	47	15	30
		105	96	49	18	29
S3	1-propanol	30	52	45	3.5	2.3
		105	54	47	3.6	1.9
		120	59	53	3.5	1.5
S4	1-butanol	10	61	53	3.8	1.9
		45	77	68	6.0	2.1
		75	88	80	6.2	1.3
		105	90	82	6.2	1.1
S5	Water	10	57	33	10	14
		90	78	45	15	18
		180	92	52	22	17
S6[c]	Acetone	45	15	4.3	2.6	8.5
		75	24	6.5	2.0	15
		105	29	9.0	2.0	20

[a] Reaction Conditions: NB (2.54 mmol, 0.42M), **Cε** (25 mg, 0.1 *mol*% of Au), $NaBH_4$ (15.2 mmol), 25°C, solvent (6 mL), N_2 protective atmosphere (1 bar). [b] Conversions and yields evaluated using GC-MS analysis with anisole as internal standard. [c] 0.2 *mol*% of Au.

Published as J. Catal. 2016, 340, 30-40. doi.org/10.1016/j.jcat.2016.05.005

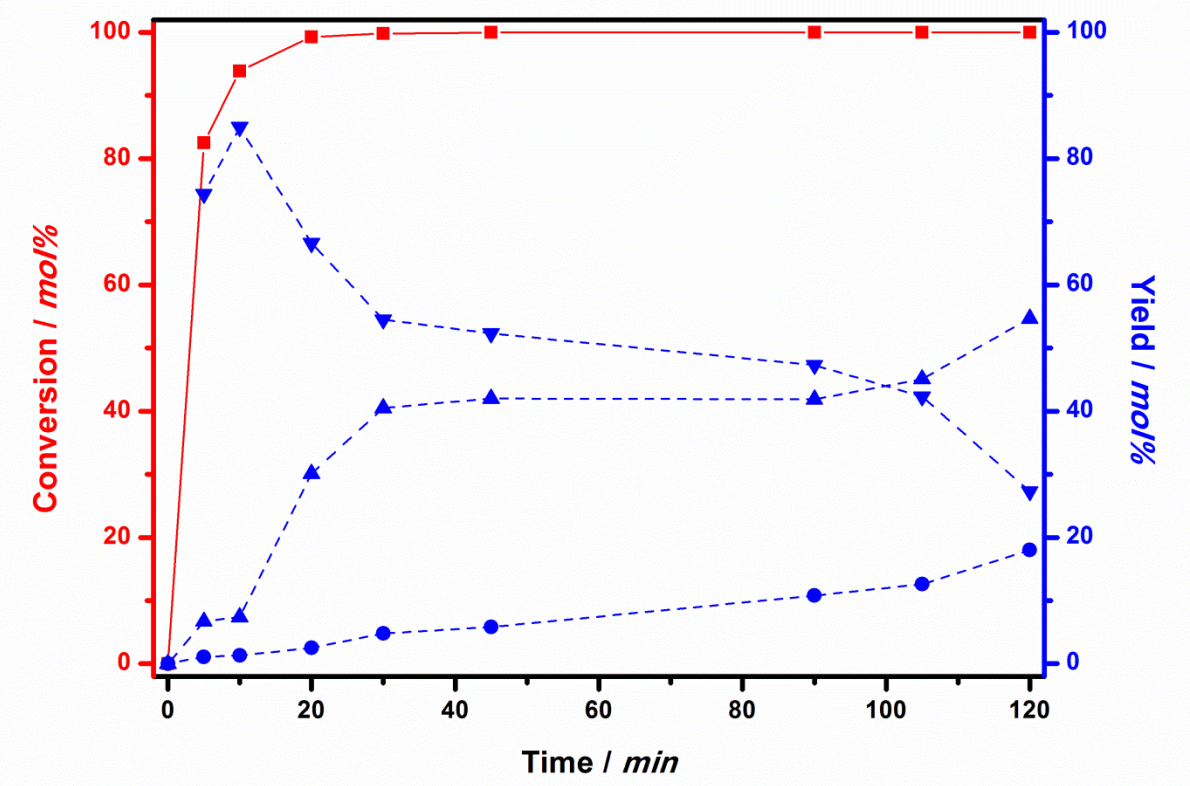

Figure S12. Reaction profile of entry **S1** of Table S15.
(■ = NB conversion; ▼= AOB yield; ▲= AB yield; ● = AN yield).

Table S9. Course of the reaction of entry **S1** of Table S15.

Time (*min*)	**NB Conversion (mole%)**	**Yield (mole%)**		
		AOB	**AB**	**AN**
5	83	74	6.7	1.1
10	94	85	7.4	1.3
20	99	67	30	2.5
30	>99	54	41	4.8
45	>99	52	42	5.8
90	>99	47	42	11
105	>99	42	45	13
120	>99	27	55	18

Reaction Conditions: NB (2.54 mmol), **Au-Cε** (25 mg; 0.1 *mol*% of Au), $NaBH_4$ (15.2 mmol), ethanol (6 mL), 25 °C, N_2 atmosphere. Conversion and yields determined by GC-MS (anisole as internal standard).

Published as J. Catal. 2016, 340, 30-40. doi.org/10.1016/j.jcat.2016.05.005

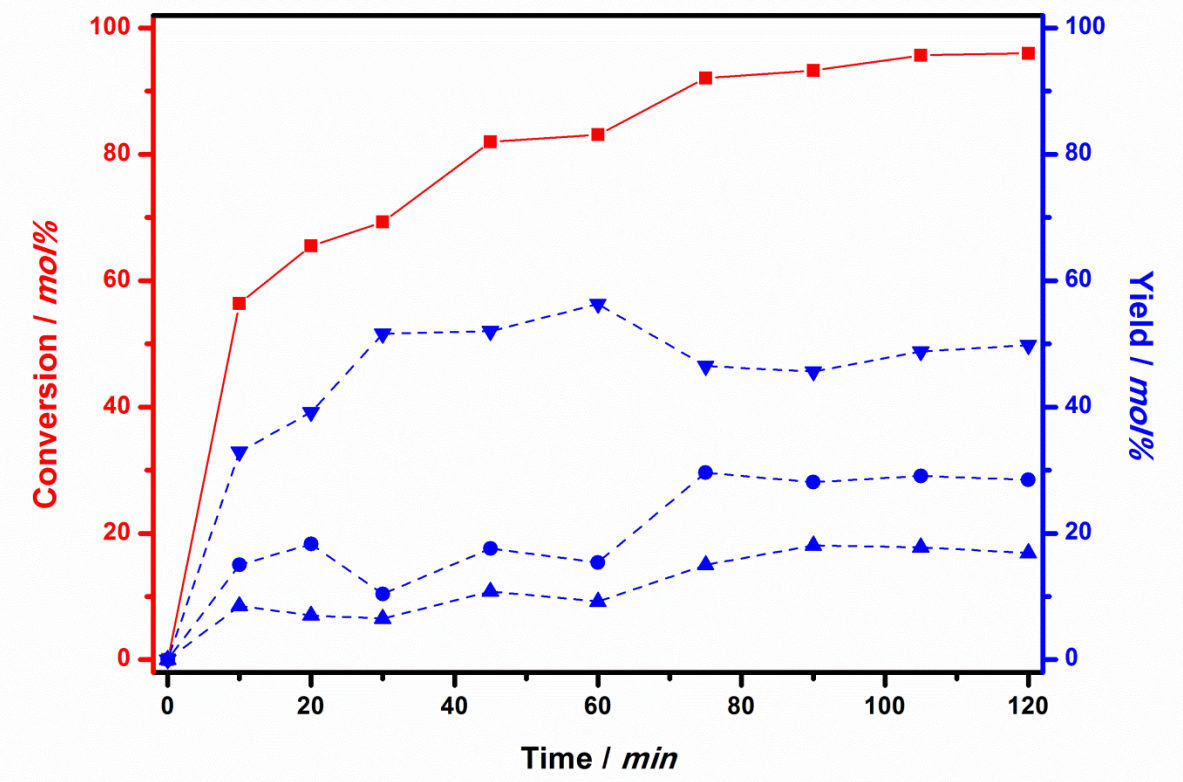

Figure S13. Reaction profile of entry **S2** of Table S15.
(■ = NB conversion; ▼= AOB yield; ▲= AB yield; ● = AN yield).

Table S10. Course of the reaction of entry **S2** of Table S15.

Time (*min*)	**NB Conversion (mole%)**	**Yield (mole%)**		
		AOB	**AB**	**AN**
10	56	33	8.0	15
20	66	39	7.0	18
30	69	52	6.5	10
45	82	52	11	18
60	83	56	8.2	15
75	92	47	15	30
90	93	46	18	28
105	96	49	18	29
120	96	50	17	29

Reaction Conditions: NB (2.54 mmol), **Au-Cε** (25 mg; 0.1 *mol*% of Au), $NaBH_4$ (15.2 mmol), ethylene glycol (6 mL), 25 °C, N_2 atmosphere. Conversion and yields determined by GC-MS (anisole as internal standard).

Published as J. Catal. 2016, 340, 30-40. doi.org/10.1016/j.jcat.2016.05.005

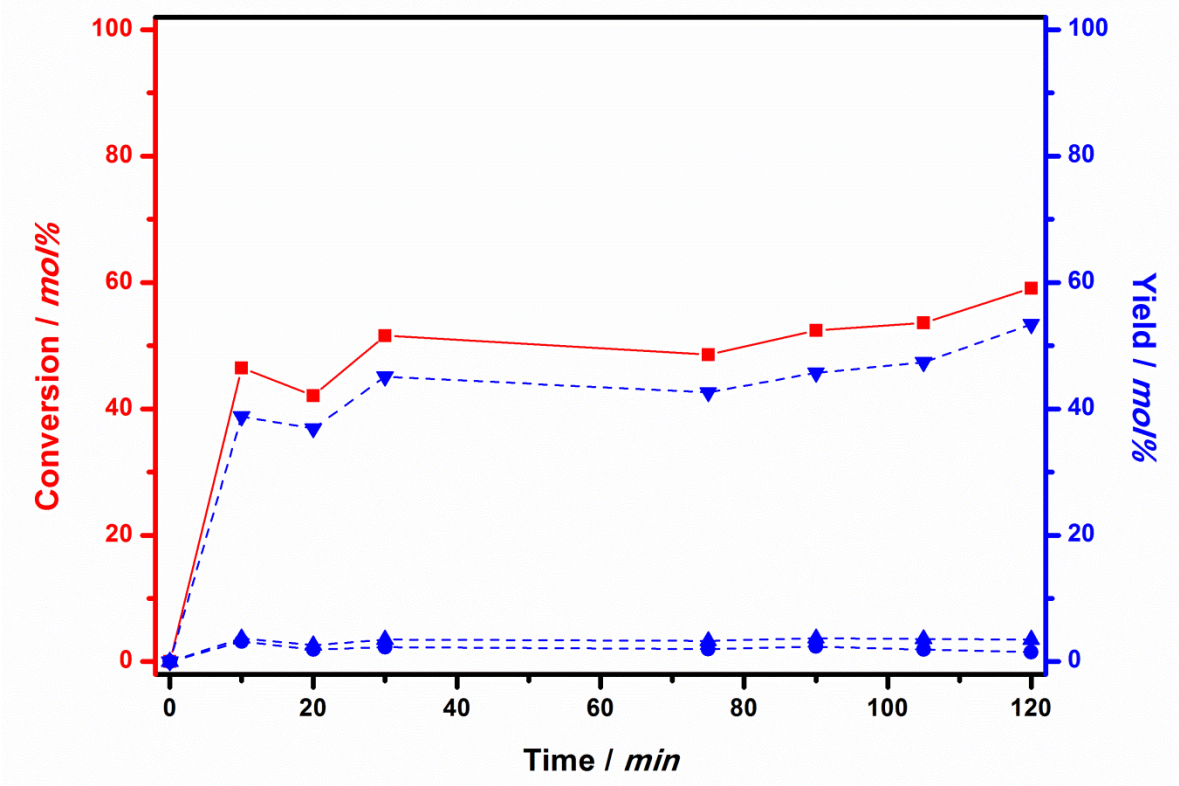

Figure S14. Reaction profile of entry **S3** of Table S15.
(■ = NB conversion; ▼= AOB yield; ▲= AB yield; ● = AN yield).

Table S11. Course of the reaction of entry **S3** of Table S15.

Time (*min*)	**NB Conversion (mole%)**	**Yield (mole%)**		
		AOB	**AB**	**AN**
10	47	39	3.7	3.2
20	42	37	2.6	1.9
30	52	45	3.5	2.3
75	49	43	3.3	2.0
90	52	46	3.6	2.4
105	54	47	3.6	1.9
120	59	53	3.5	1.5

Reaction Conditions: NB (2.54 mmol), **Au-Cε** (25 mg; 0.1 *mol%* of Au), $NaBH_4$ (15.2 mmol), 1-propanol (6 mL), 25 °C, N_2 atmosphere. Conversion and yields determined by GC-MS (anisole as internal standard).

Published as J. Catal. 2016, 340, 30-40. doi.org/10.1016/j.jcat.2016.05.005

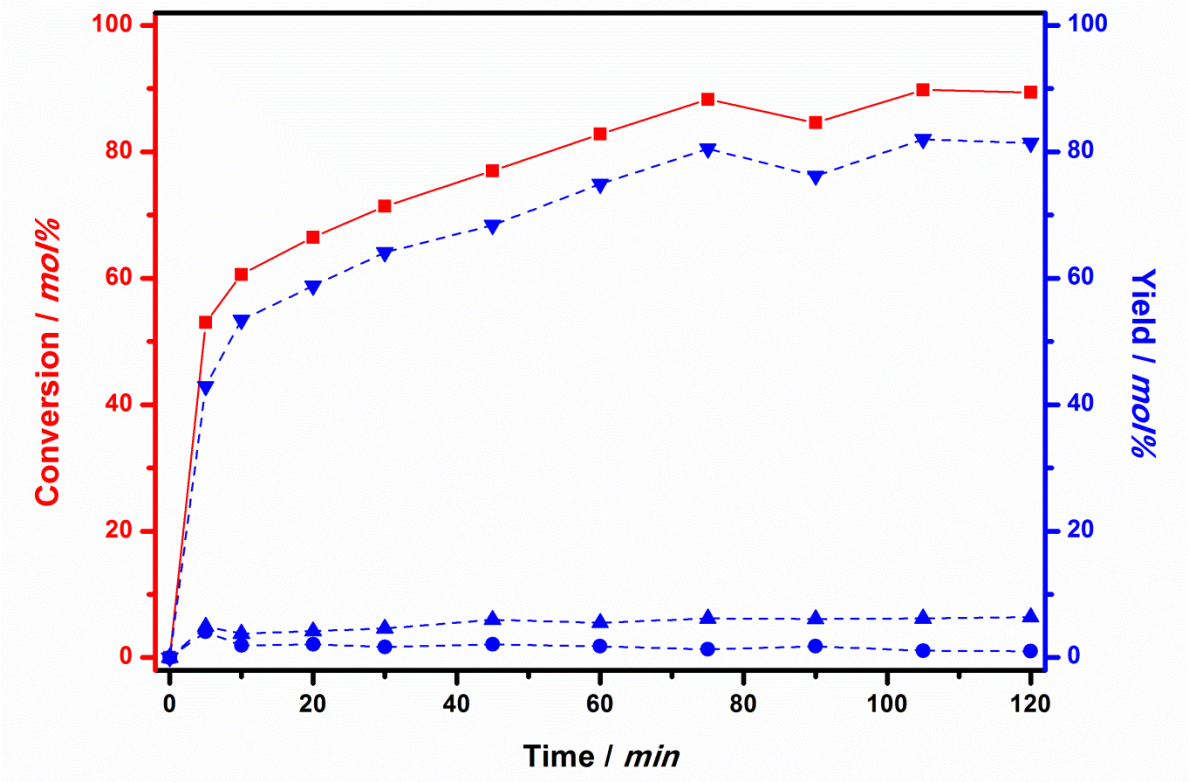

Figure S15. Reaction profile of entry **S4** of Table S15.
(■ = NB conversion; ▼= AOB yield; ▲= AB yield; ● = AN yield).

Table S12. Course of the reaction of entry **S4** of Table S15.

Time (*min*)	**NB Conversion (mole%)**	**Yield (mole%)**		
		AOB	**AB**	**AN**
5	53	43	4.9	4.1
10	61	53	3.8	1.9
20	67	59	4.2	2.1
30	71	64	4.6	1.7
45	77	68	6.0	2.1
60	83	75	5.5	1.8
75	88	80	6.2	1.3
90	85	76	6.1	1.8
105	90	82	6.2	1.1
120	89	81	6.4	1.0

Reaction Conditions: NB (2.54 mmol), **Au-Cε** (50 mg; 0.2 *mol*% of Au), $NaBH_4$ (15.2 mmol), 1-butanol (6 mL), 25 °C, N_2 atmosphere. Conversion and yields determined by GC-MS (anisole as internal standard).

Published as J. Catal. 2016, 340, 30-40. doi.org/10.1016/j.jcat.2016.05.005

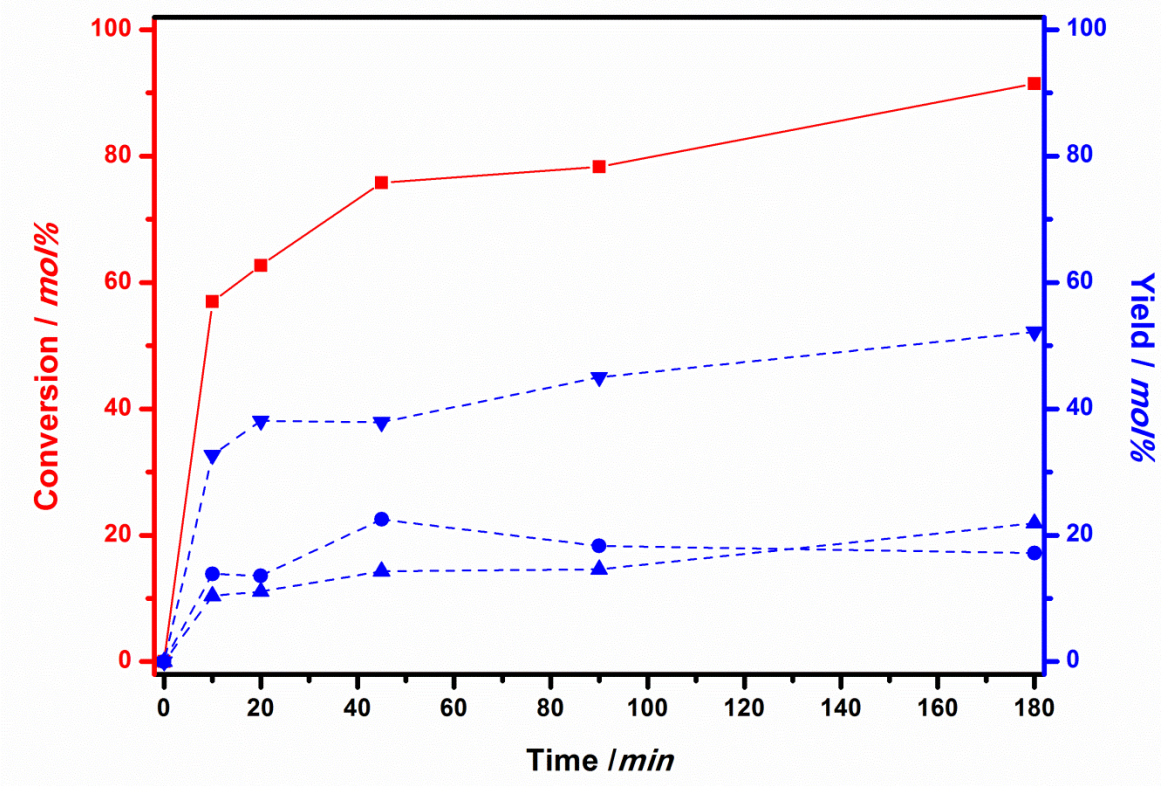

Figure S16. Reaction profile of entry **S5** of Table S15.
(■ = NB conversion; ▼= AOB yield; ▲= AB yield; ● = AN yield).

Table S13. Course of the reaction of entry **S5** of Table S15.

Time (*min*)	**NB Conversion (mole%)**	**Yield (mole%)**		
		AOB	**AB**	**AN**
0	0	0	0	0
10	57	33	10	14
20	63	38	11	14
45	76	38	14	23
90	78	45	15	18
180	92	52	22	17

Reaction Conditions: NB (2.54 mmol), **Au-Cε** (25 mg; 0.1 mole% of Au), $NaBH_4$ (15.2 mmol), D_2O (6 mL), 25 °C, N_2 atmosphere. Conversion and yields determined by GC-MS (anisole as internal standard).

Published as J. Catal. 2016, 340, 30-40. doi.org/10.1016/j.jcat.2016.05.005

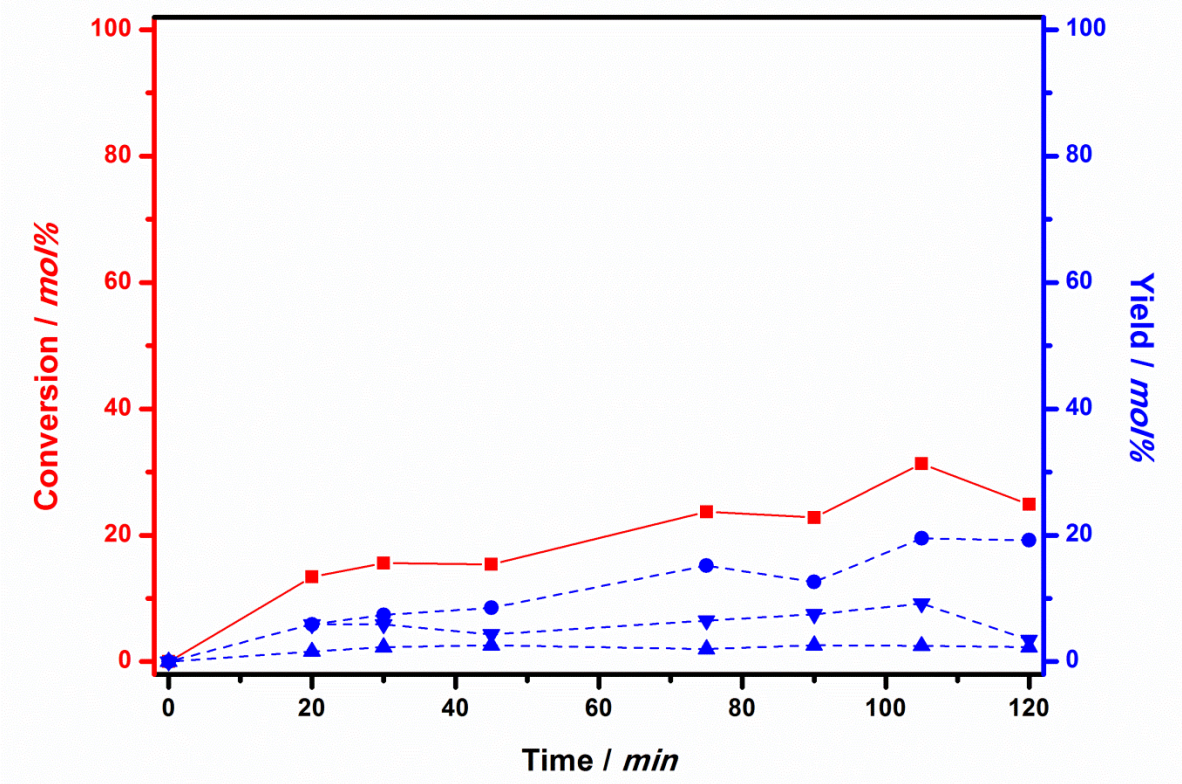

Figure S17. Reaction profile of entry **S6** of Table S15.
(■ = NB conversion; ▼= AOB yield; ▲= AB yield; ● = AN yield).

Table S14. Course of the reaction of entry **S6** of Table S15.

Time (*min*)	**NB Conversion (mole%)**	**Yield (mole%)**		
		AOB	**AB**	**AN**
20	13	5.5	1.6	5.9
30	16	5.9	2.3	7.4
45	15	4.3	2.5	8.5
75	24	6.5	2.0	15
90	23	7.5	2.6	13
105	31	9.0	2.0	20
120	25	3.4	2.3	19

Reaction Conditions: NB (2.54 mmol), **Au-Cε** (25 mg; 0.1 mole% of Au), $NaBH_4$ (15.2 mmol), acetone (6 mL), 25 °C, N_2 atmosphere. Conversion and yields determined by GC-MS (anisole as internal standard).

Published as J. Catal. 2016, 340, 30-40. doi.org/10.1016/j.jcat.2016.05.005

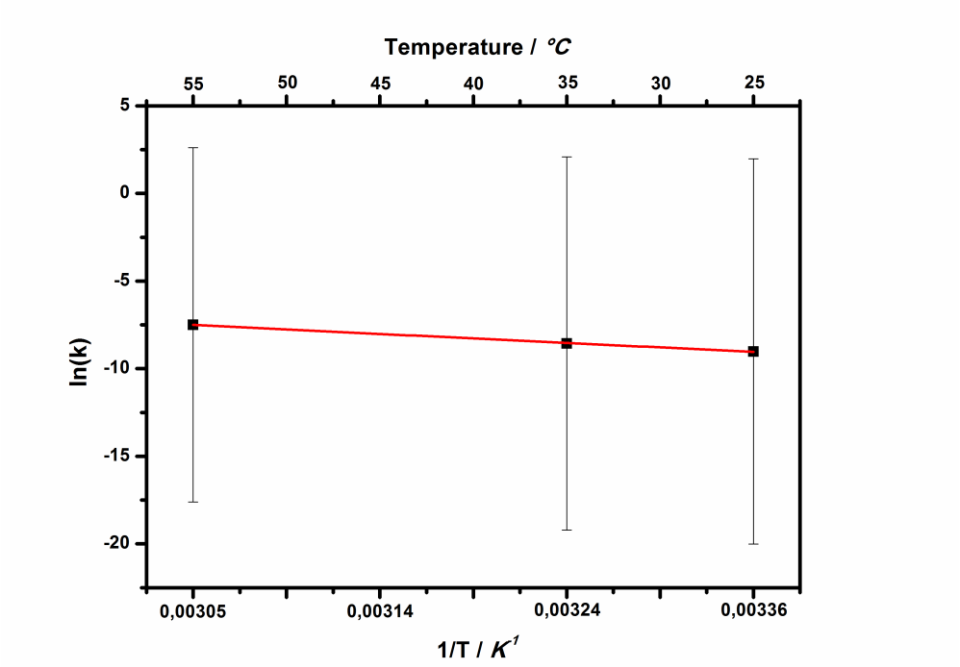

Figure S18. Arrhenius plot for the formation of aniline from entries **4** (Table 1), **1** and **3** (Table 2).

Published as J. Catal. 2016, 340, 30-40. doi.org/10.1016/j.jcat.2016.05.005

3. Reutilization of the Catalyst Au-Cε.

Table S15. Reutilization of the catalyst **Au-Cε**.

Use[a]	**NB Conversion**[b] **(*mol%*)**	**AN Selectivity**[b] **(*mol%*)**	**TOF**[c] **(h^{-1})**
1st	>99	>99	500
2nd	>99	>99	500
3rd	>99	97	485
4th	>99	>99	500

[a] Reaction Conditions: NB (2.54 mmol), **Au-Cε** (50 mg; 0.2 *mol*% of Au), $NaBH_4$ (15.2 mmol), MeOH (6 mL), 25 °C, N_2 atmosphere; 1 h. Conversion and selectivity determined by GC-MS (anisole as internal standard). [c] Turnover frequency at 1 h.